JACS
JOURNAL OF THE AMERICAN CHEMICAL SOCIETY
pubs.acs.org/JACS
Article

Strongly Red-Emissive Molecular Ruby $[Cr(bpmp)_2]^{3+}$ Surpasses $[Ru(bpy)_3]^{2+}$

Florian Reichenauer, Cui Wang, Christoph Förster, Pit Boden, Naz Ugur, Ricardo Báez-Cruz, Jens Kalmbach, Luca M. Carrella, Eva Rentschler, Charusheela Ramanan, Gereon Niedner-Schatteburg, Markus Gerhards, Michael Seitz,* Ute Resch-Genger,* and Katja Heinze*

Cite This: J. Am. Chem. Soc. 2021, 143, 11843−11855
Read Online
ACCESS | Metrics & More | Article Recommendations | Supporting Information

ABSTRACT: Gaining chemical control over the thermodynamics and kinetics of photoexcited states is paramount to an efficient and sustainable utilization of photoactive transition metal complexes in a plethora of technologies. In contrast to energies of charge transfer states described by spatially separated orbitals, the energies of spin-flip states cannot straightforwardly be predicted as Pauli repulsion and the nephelauxetic effect play key roles. Guided by multi-reference quantum chemical calculations, we report a novel highly luminescent spin-flip emitter with a quantum chemically predicted blue-shifted luminescence. The spin-flip emission band of the chromium complex $[Cr(bpmp)_2]^{3+}$ (bpmp = 2,6-bis(2-pyridyl-methyl)pyridine) shifted to higher energy from ca. 780 nm observed for known highly emissive chromium(III) complexes to 709 nm. The photoluminescence quantum yields climb to 20%, and very long excited state lifetimes in the millisecond range are achieved at room temperature in acidic D_2O solution. Partial ligand deuteration increases the quantum yield to 25%. The high excited state energy of $[Cr(bpmp)_2]^{3+}$ and its facile reduction to $[Cr(bpmp)_2]^{2+}$ result in a high excited state redox potential. The ligand's methylene bridge acts as a Brønsted acid quenching the luminescence at high pH. Combined with a pH-insensitive chromium(III) emitter, ratiometric optical pH sensing is achieved with single wavelength excitation. The photophysical and ground state properties (quantum yield, lifetime, redox potential, and acid/base) of this spin-flip complex incorporating an earth-abundant metal surpass those of the classical precious metal $[Ru(\alpha\text{-diimine})_3]^{2+}$ charge transfer complexes, which are commonly employed in optical sensing and photo(redox) catalysis, underlining the bright future of these molecular ruby analogues.

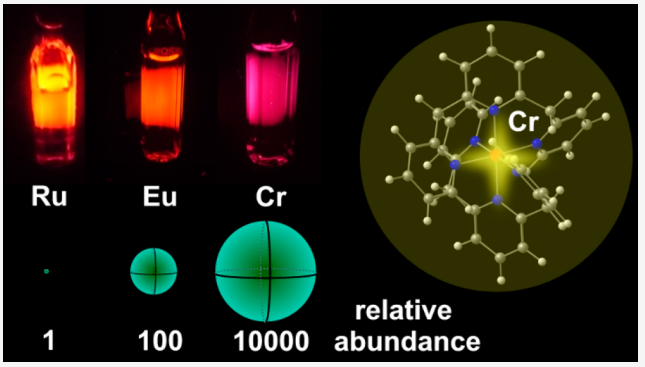

INTRODUCTION

In optical sensing, imaging, and photo(redox) chemistry, complexes with d^6 (e.g., Ru^{II}, Ir^{III}, Os^{II}, or Re^{I} and recently Mo^0),[1−13] d^8 (Pt^{II}, Au^{III}),[14] or d^{10} (Cu^{I})[15−22] electron configuration and electron deficient ligands are typically employed. Complexes of these metal ions with suitable electron accepting ligands such as 2,2′-bipyridine (bpy) or 2,2′:6′,2″-terpyridine (tpy) can possess favorable long-lived, luminescent, and/or redox active triplet metal-to-ligand charge transfer (^{3}MLCT) states. Such complexes are hence ubiquitous in photosensitized reactions, OLEDs, bioimaging probes, optical sensors, photodrugs, and dye-sensitized solar cells.[1−10] In the past few years, the substitution of precious metals by earth-abundant base metals has become a vivid and important research area aiming at sustainable photochemistry and photophysical applications.[23−40] Luminescent ligand-to-metal (LMCT) states of earth-abundant Fe^{III} and Co^{III} complexes have emerged very recently as alternative useful excited states of 3d transition metal complexes.[38−40] The highest quantum yields achieved so far with charge transfer (CT) emitters of MLCT or LMCT character based on earth-abundant 3d metals (except from the special case of copper(I)) are 0.001% (Cr^0),[33] 0.7% (Co^{III}),[40] and 2.1% (Fe^{III}).[38]

Fundamentally different from charge transfer states, which involve spatially separated metal and ligand frontier orbitals,[41] are metal-centered spin-flip states.[26,42−48] Such localized spin-flip states can be phosphorescent, in particular in the near-infrared spectral region.[26,44,49] These excited states could be useful for optical applications (sensing, imaging, and lasing) as well as excited state electron and energy transfer reactions. However, most transition metal complexes with a d^2 or d^3 electron configuration suitable for a spin-flip luminescence[50] are only weakly emissive ($\Phi \ll 0.15\%$).[44,49] With the development

Received: June 9, 2021
Published: July 23, 2021

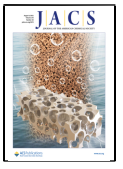

https://doi.org/10.1021/jacs.1c05971
J. Am. Chem. Soc. 2021, 143, 11843−11855

of the so-called molecular ruby $[Cr(ddpd)_2]^{3+}$ (ddpd = *N*,*N*′-dimethyl-*N*,*N*′-dipyridine-2-ylpyridine-2,6-diamine[51,52]), we achieved record photoluminescence quantum yields of Φ = 11% (Φ = 30% with a partially deuterated ddpd ligand) of the NIR luminescence (λ_{em} = 775 nm).[53,54] Several applications in the fields of sensing, photocatalysis, upconversion, and circularly polarized luminescence already emerged in the past few years.[55−64] Variations of the ligand and the complex symmetry increased the lifetime of the luminescent excited spin-flip state up to the current record value of 4500 μs.[65] However, all these highly emissive chromium(III) complexes based on the molecular ruby motif emit in the near-infrared spectral region (≫700 nm; ≪1.77 eV) up to now (Scheme 1).[53−65]

Scheme 1. NIR-Emissive Chromium(III) Complexes and Classical Red-Emissive Complexes Based on Ruthenium(II) and Europium(III)

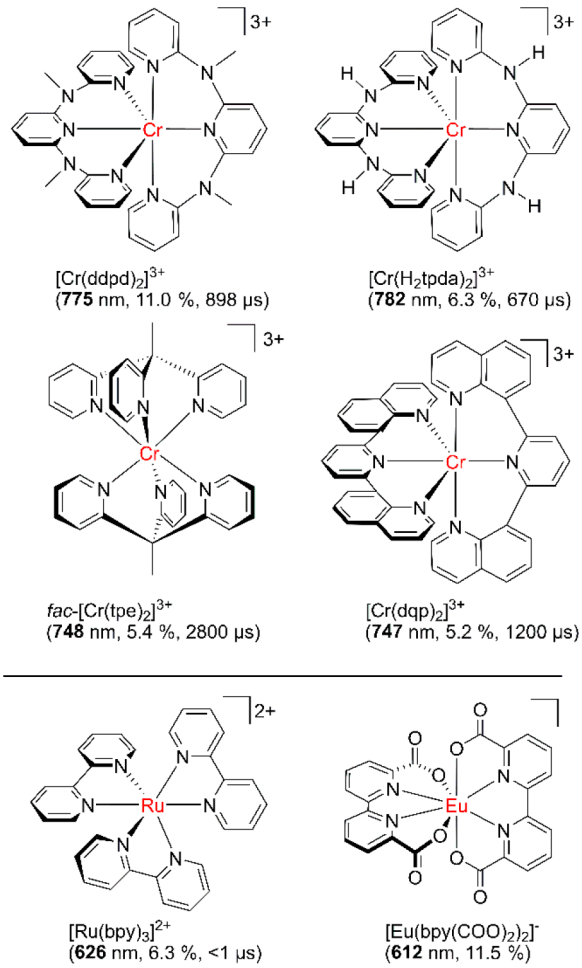

Red, long-lived emission (i.e., <≈700 nm) has been achieved by using europium(III)[66,67] and ruthenium(II) complexes (Scheme 1). Consequently, complexes of these metals are heavily exploited for example in biosensing.[68−70,48] However, these metals are dramatically less abundant than chromium by factors of ca. 100 and 10000. This scarcity is also reflected by the prices of ca. 30, 7300, and 16250 € mol^{-1} for $CrCl_3$, $EuCl_3$, and $RuCl_3$, respectively (based on the hydrated chlorides; commercial supplier, May 2021). Bright red emission from spin-flip excited states has only been realized in solid Cr^{III} materials such as ruby $Al_2O_3:Cr^{3+}$ itself (695 nm)[71−74] and in Mn^{IV}-doped solids, e.g., $K_2SiF_6:Mn^{4+}$ (630 nm),[75] but remained elusive for molecular chromium(III) complexes. Either the spin-flip states of previously reported molecular Cr^{III} complexes are at a too low energy as in the molecular rubies (Scheme 1),[53,57,64,65] or the quantum yields are extremely poor (0.024%−0.000005%).[49]

Unlike the straightforward and well-founded correlations elucidated for charge transfer complexes with MLCT, LMCT, or LL′CT excited states and organic emitters with donor−acceptor character, shifting of the excited doublet state levels of such spin-flip emitters and hence the emission color by chemical measures, such as donor atom variation or substitution patterns of the ligands, is extremely difficult to predict. A clear-cut correlation with ligand types for chromium(III) spin-flip emitters[49] remains elusive beyond the classical ligand field parameters of the covalently reduced d−d interelectronic repulsion (*B* and *C* ligand field parameters), that is, the nephelauxetic series of simple classical ligands such as halides.[76−78] The accurate description[79−82] of the relevant excited quartet *and* doublet states[83−86,58] is challenging due to the required consideration of interelectronic repulsion.[81] The localized spin-flip character instead of the charge transfer nature of the classical CT luminophores with separately addressable spatially distinct wave functions has furthermore precluded reliable predictions for spin-flip levels so far. However, recent method developments in quantum chemistry and coding suitable for open-shell complexes of realistic size in general and chromium(III) in particular conceptually tackled this challenge.[79−87]

In this study, we address the challenge to increase the energy of the spin-flip state in molecular chromium(III) complexes, while concomitantly maintaining a high quantum yield by providing a large enough energy gap between the detrimental metal centered quartet states and the emissive spin-flip level(s) using high-level quantum chemical calculations and the translation to synthesis, spectroscopy, and first applications of the resulting complex.

RESULTS AND DISCUSSION

Quantum Chemical Screening. To identify a ligand modification, which shifts the energy of the emissive spin-flip state(s) (^2E and $^2T_1$) of chromium(III) complexes to higher energy while maintaining a large enough quartet state energy ($^4T_2$), we screened six-coordinate chromium(III) complexes with several monodentate and chelate ligands (NH_3, CN^-, $acac^-$) and in particular pyridine-based ligands (py, bpy, tpy, ddpd) by high-level quantum chemical methods. As density functional theory (DFT) methods failed to give the correct ordering of doublet (^2E, $^2T_1$) and quartet excited states ($^4T_2$),[81] an ab initio multireference method was selected.[83−86] Complete active space self-consistent field (CASSCF) calculations combined with *N*-electron valence state perturbation theory (NEVPT2) to account for dynamic electron correlation based on a fully internally contracted (FIC) wave function have been successfully used for open-shell metal complexes.[83−86,58,44] This method was employed in the following for the complexes selected.

First, DFT calculations on the CPCM(acetonitrile)-UB3LYP-D3BJ-ZORA/def2-TZVPP level deliver the optimized geometries of the chromium(III) complexes in their respective $^4A_2$ ground states. Subsequently, CASSCF-FIC-NEVPT2 calculations with an active space comprising the five 3d orbitals and the three d electrons CAS(3,5) estimate the required excited state energies (Table S1, Supporting Information). These calcu-

https://doi.org/10.1021/jacs.1c05971
J. Am. Chem. Soc. 2021, 143, 11843−11855

lations were followed by an ab initio ligand field theory (AILFT) analysis to yield the Racah parameters B and C and the ligand field splitting Δ_0 (Table S2).[83,84]

This initial screening of DFT-optimized chromium(III) complexes coordinated by monodentate and chelate ligands $Cr(acac)_3$, $[Cr(NH_3)_6]^{3+}$, $[Cr(py)_6]^{3+}$, $[Cr(tpy)_2]^{3+}$, $[Cr(bpy)_3]^{3+}$, $[Cr(ddpd)_2]^{3+}$, and $[Cr(CN)_6]^{3-}$ yielded ligand field splittings Δ_0 ($^4T_2$ energies) increasing in the order of $acac^-$ < py < tpy < ddpd < NH_3 < bpy < CN^- (Table S1). The experimental spectrochemical series $acac^-$ < tpy < ddpd < bpy < CN^-, that is, the experimentally observed ligand field transitions $^4A_2 \rightarrow {}^4T_2$, confirms this approach. As the ligand field splitting Δ_0 of all these complexes is large enough to enable luminescence from doublet states, the decisive parameter is the Racah parameter B, which determines the energy of the doublet states. The calculated B values increase in the order CN^- (888 cm^{-1}) < tpy < ddpd < py < $acac^-$ ≈ bpy < NH_3 (988 cm^{-1}) (Table S2). Clearly, this nephelauxetic series is difficult to explain or even to predict based on simple guidelines. As the tridentate ddpd ligand performed well in previous luminescence studies of its chromium(III) complex due to its large enough Δ_0 and relative rigidity,[26,53,54] we attempted simple modifications of ddpd maintaining the tridentate ligation and the six-membered chelate rings.

Replacing the NMe groups of the ddpd ligand by CH_2 bridges provided a hit structure based on the two conditions of high energy doublet *and* high energy excited quartet levels. The chromium(III) complex $[Cr(bpmp)_2]^{3+}$ with the ligand 2,6-bis(2-pyridylmethyl)pyridine (bpmp) shows the highest calculated B = 1003 cm^{-1} in the series, while maintaining a large enough Δ_0 = 20882 cm^{-1} (Tables S1 and S2).

For $[Cr(bpmp)_2]^{3+}$ and its parent complex $[Cr(ddpd)_2]^{3+}$ the active space was then expanded to CAS(7,12) with the two filled Cr−N σ-bonding orbitals and a second d shell.[86,87] This methodology had proven to be sufficiently accurate to predict the relative energies of excited quartet and doublet states and even the energy gap between the two lowest doublet states for $[Cr(ddpd)_2]^{3+}$.[58]

The refined calculation of the doublet and quartet excited states of $[Cr(bpmp)_2]^{3+}$ using CASSCF(7,12)-FIC-NEVPT2 confirmed the relative doublet and quartet energies (Figure 1; Tables S1 and S3). Interestingly, one doublet microstate of $^2T_1$ parentage drops below the lowest energy doublet microstate of ^2E parentage in the CASSCF(7,12)-FIC-NEVPT2 calculation, similar to the doublet state ordering of the parent complex $[Cr(ddpd)_2]^{3+}$ (Figure 1 and Table S3).[58] The energy gap between the lowest doublet state and the lowest excited quartet level (from the $^4T_2$ set) in $[Cr(bpmp)_2]^{3+}$ amounts to 6010 cm^{-1} (>70 kJ mol^{-1}) on this level of theory. After excitation, intersystem crossing (ISC), and vibrational cooling (VC), this large gap prohibits back-intersystem crossing (back-ISC) at room temperature. Consequently, the detrimental nonradiative relaxation via the $^4T_2$ state is eliminated. Importantly, the calculated energy of the lowest emissive doublet level of $[Cr(bpmp)_2]^{3+}$ exceeds that calculated for $[Cr(ddpd)_2]^{3+}$ by 766 cm^{-1} at the same level of theory as desired (Figure 1 and Table S3).

Synthesis, Structure, and Ground State Reactivity of $[Cr(bpmp)_2]^{3+}$. Encouraged by the quantum chemical predictions and the facile synthesis of the proposed suitable ligand bpmp,[88] the corresponding chromium(III) complex $[Cr(bpmp)_2]^{3+}$ was prepared. However, unlike the straightforward synthesis of $[Cr(ddpd)_2]^{3+}$,[53] simple mixing of bpmp and

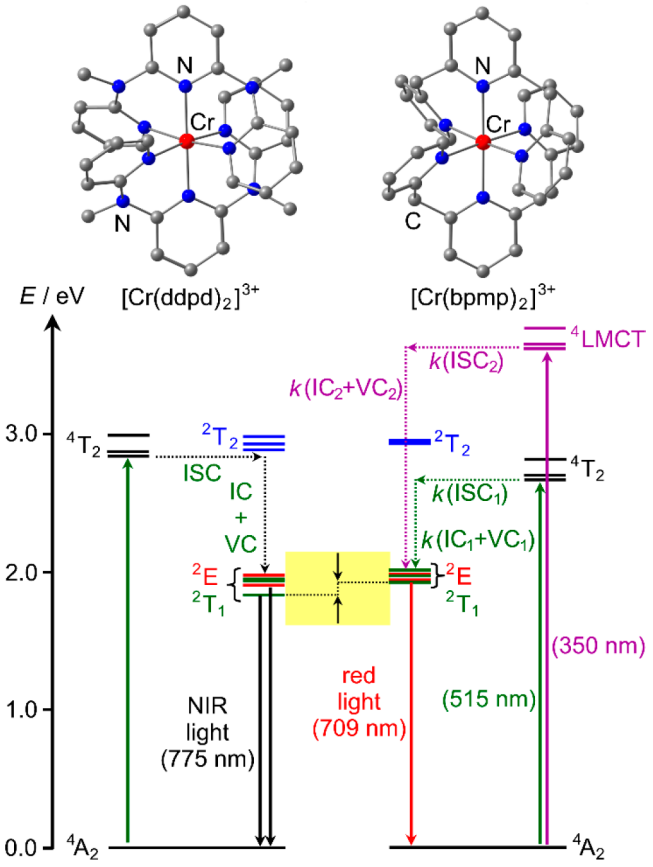

Figure 1. DFT-optimized geometries and Jablonski diagrams derived from CASSCF(7,12)-FIC-NEVPT2 calculations of $[Cr(ddpd)_2]^{3+}$ (left)[58] and $[Cr(bpmp)_2]^{3+}$ (right). The energy difference between the two lowest doublet levels of the complexes is indicated by arrows and highlighted in yellow. ISC = intersystem crossing, IC = internal conversion, and VC = vibrational cooling. Decay cascades starting from ^{4}LMCT and $^4T_2$ states are indicated with dotted purple and green arrows, respectively. The experimentally employed excitation and observed emission wavelengths are given in parentheses.

$CrCl_2$ resulted in redox reactions instead of the desired complexation. Consequently, a stepwise route starting from chromium(III) chloride[89,90] instead of chromium(II) chloride was applied (Figure 2a).

Refluxing the inexpensive starting material $CrCl_3 \cdot 6H_2O$ with 1 equiv of the ligand bpmp in isopropanol gives the green chlorido complex $Cr(bpmp)Cl_3$ in nearly quantitative yield (Figure 2a). The heteroleptic complex $Cr(bpmp)Cl_3$ was characterized by IR spectroscopy, mass spectrometry, and elemental analysis (Figures S1 and S2). Quantitative substitution of the three coordinated chlorido ligands of $Cr(bpmp)Cl_3$ by more labile triflates with triflic acid yields the red-brown complex $Cr(bpmp)(OTf)_3$ under release of gaseous HCl (Figure 2a). An analogous procedure starts from $CrBr_3 \cdot 6H_2O$ but gives no further advantage (Figures S3 and S4). The constitution of $Cr(bpmp)(OTf)_3$ is confirmed by IR spectroscopy, mass spectrometry, and single crystal X-ray diffraction (Figure 2b, Figures S5 and S6).

XRD analysis of a single crystal of $Cr(bpmp)(OTf)_3 \cdot {}^1/_4CH_3CN$ confirms the meridional configuration of the cation (Figure 2b). Interestingly, the triflato ligands form intra- and intermolecular CH···O hydrogen bonds to the methylene bridges of the bpmp ligand, indicating a significant

https://doi.org/10.1021/jacs.1c05971
J. Am. Chem. Soc. 2021, 143, 11843−11855

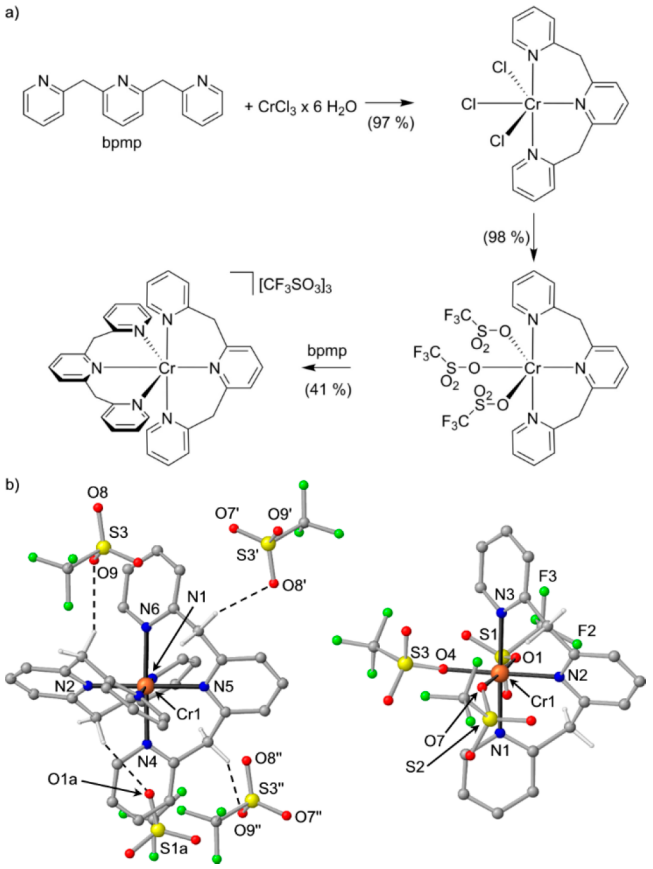

Figure 2. (a) Synthesis of $[Cr(bpmp)_2][OTf]_3$ via $Cr(bpmp)Cl_3$ and $Cr(bpmp)(OTf)_3$ and (b) molecular structures of the complexes in the solid state. Hydrogen bonding of triflate ions to the CH_2 groups is illustrated in $[Cr(bpmp)_2][OTf]_3$ by dashed lines. Hydrogen atoms (except for the CH_2 groups) are omitted.

CH acidity of the coordinated ligand ($d(C\cdots O_{intra})$ = 3.00−3.36 Å; $d(C\cdots O_{inter})$ = 3.52−3.56 Å). Ligand exchange by a further equivalent of bpmp furnishes the cationic paramagnetic orange complex as triflate salt $[Cr(bpmp)_2][OTf]_3$ (Figure 2a) substantiated by IR spectroscopy, mass spectrometry, elemental analysis, and SQUID magnetometry (Figures S7−S9). Its constitution and meridional configuration was confirmed by single crystal X-ray diffraction of $[Cr(bpmp)_2][OTf]_3 \cdot CH_3CH_2OH$ (Figure 2b and Table S6).

The experimental structure of the cation fits to the geometry calculated by DFT (Figures 1 and 2b, Table S6). Notably, the $[CrN_6]$ core is highly octahedral with balanced Cr−N distances and N−Cr−N angles close to 90°. This ensures a large Cr/N orbital overlap and consequently a large ligand field splitting and high energy excited quartet levels.

In the solid state, the methylene bridges of the bpmp ligands form CH···O hydrogen bonds with the triflate counterions ($d(C\cdots O)$ = 3.12−3.49 Å; Figure 2b) similar to $Cr(bpmp)(OTf)_3$. Exchange of the triflates could be achieved with $[^nBu_4N][BF_4]$, $[^nBu_4N][PF_6]$, or $[^nBu_4N][ClO_4]$ as shown by IR spectroscopy, mass spectrometry, elemental analysis, and single crystal XRD analysis of the tetrafluoroborate salt (Figures S10−S14). Hydrogen bonds of the ligand's CH_2 bridges to BF_4^- counterions are present with C···F distances between 2.90 and 3.70 Å in the solid state (Figure S14).

At pH above 7−8, $[Cr(bpmp)_2]^{3+}$ converts to a dark yellow to brown complex in solution (Video S1). Even a solid sample reacts with gaseous ammonia to the brown complex and back to starting material with gaseous HCl (Video S2). UV/vis spectroscopy in H_2O reveals intense broad bands at ca. 350, 455, 540, 615, and 730 nm tailing up to 950 nm (Figure S15). This reactivity is associated with the acidity of the bridging CH_2 units in the cationic complex, which is already reflected in the hydrogen bonding of the triflates to the CH_2 groups in the solid state (Figure 2b). Comparing the experimental UV/vis spectrum with the time-dependent (TD-)DFT calculated transitions for the corresponding base $[Cr(bpmp)(bpmp\text{-}H)]^{2+}$ supports this acid/base chemistry (Figure S15 and Table S7). Photometric titration yields a pK_a value of 8.6 (Figure S16). $[Cr(bpmp)_2]^{3+}$ is similarly acidic as the NH analogue $[Cr(H_2tpda)_2]^{3+}$ with NH bridging units (pK_a 8.8; Scheme 1).[57] The methylene bridge can be reversibly de- and reprotonated by NaOH and HCl_{aq} or HOTf, respectively, several times as demonstrated optically and photometrically (Figure S17). However, above ca. pH 10 further processes set in which are partially irreversible, as suggested by the optical spectra (Figure S17). ESI mass spectra of $[Cr(bpmp)_2][OTf]_3$ display peaks at mass-to-charge ratios of 191.4 (7%), 286.6 (13%), and 572.2 (100%), corresponding to $\{[Cr(bpmp)_2]\}^{3+}$, $\{[Cr(bpmp)_2]\text{-}H\}^{2+}$, and $\{[Cr(bpmp)_2]\text{-}2H\}^{+}$, respectively (Figure S7). The BF_4^- and PF_6^- salts exhibits similar mass spectroscopic patterns (Figures S10 and S12). This further underscores the high acidity of $[Cr(bpmp)_2]^{3+}$. To ensure full protonation of the bridge and prohibit any decomposition, pertinent optical measurements were performed in the presence of aqueous perchloric acid.

A reversible $[Cr(bpmp)_2]^{3+/2+}$ reduction wave appears at −0.81 V vs ferrocene in the cyclic voltammogram followed by the waves for the $[Cr(bpmp)_2]^{2+/+}$, $[Cr(bpmp)_2]^{+/0}$, and $[Cr(bpmp)_2]^{0/1-}$ couples at −1.80, −2.13, and −2.31 V, respectively (Figures S18 and S19). The $[Cr(bpmp)_2]^{3+/2+}$ wave is shifted anodically by 0.3 V compared to that of the $[Cr(ddpd)_2]^{3+/2+}$ couple.[53] The more electron-deficient nature of the bpmp ligand as compared to ddpd accounts for this redox potential shift. Indeed, DFT calculations of $[Cr(bpmp)_2]^{2+}$ suggest an electronic structure of a low-spin chromium(II) ion admixed with a chromium(III) ion antiferromagnetically coupled to a ligand-centered radical (Figure S20). With this assignment, the electronic structure of $[Cr(bpmp)_2]^{2+}$ is between a genuine chromium(II) ion as found for $[Cr(ddpd)_2]^{2+}$ [53,93] and a ligand-centered radical found for $[Cr(bpy)_3]^{2+}/[Cr(tpy)_2]^{2+}$ [91,92] and $[Cr(tpe)_2]^{2+}$ [65] complexes (Figure 1, tpe = 1,1,1-tris(pyrid-2-yl)ethane).

Excited State Properties and Dynamics. The absorption spectrum of $[Cr(bpmp)_2]^{3+}$ in solution (H_2O or CH_3CN) can be divided into three spectral regions (Figure 3a). According to TD-DFT calculations (Figure S21), bands at 239 and 270 nm are assigned to $\pi-\pi^*$ transitions of the ligand, the band at 340 nm to ^{4}LMCT transitions, and the weak band at 465 nm (ε = 60 M^{-1} cm^{-1}, Figure 3a) to Laporte-forbidden $^4A_2 \rightarrow {}^4T_2$ transitions.

The latter absorption band reflects the ligand field splitting ($\Delta_{0,exp} \approx 21500$ cm^{-1}). This splitting is somewhat smaller than that of $[Cr(ddpd)_2]^{3+}$ with $\Delta_{0,exp} \approx 22990$ cm^{-1}.[53] The CASSCF-NEVPT2 calculations confirm this smaller ligand field splitting (Figure 1). The splitting is still sufficiently large to prevent nonradiative decay via back-ISC. Yet, this lower energy for excitation might be beneficial for future applications. Excitation with 462 nm light gives rise to a very sharp emission band (FWHM 280 cm^{-1}) peaking at 709 nm (Figure 3a). This is at the lower energy side of the visible spectral region giving a

https://doi.org/10.1021/jacs.1c05971
J. Am. Chem. Soc. 2021, 143, 11843−11855

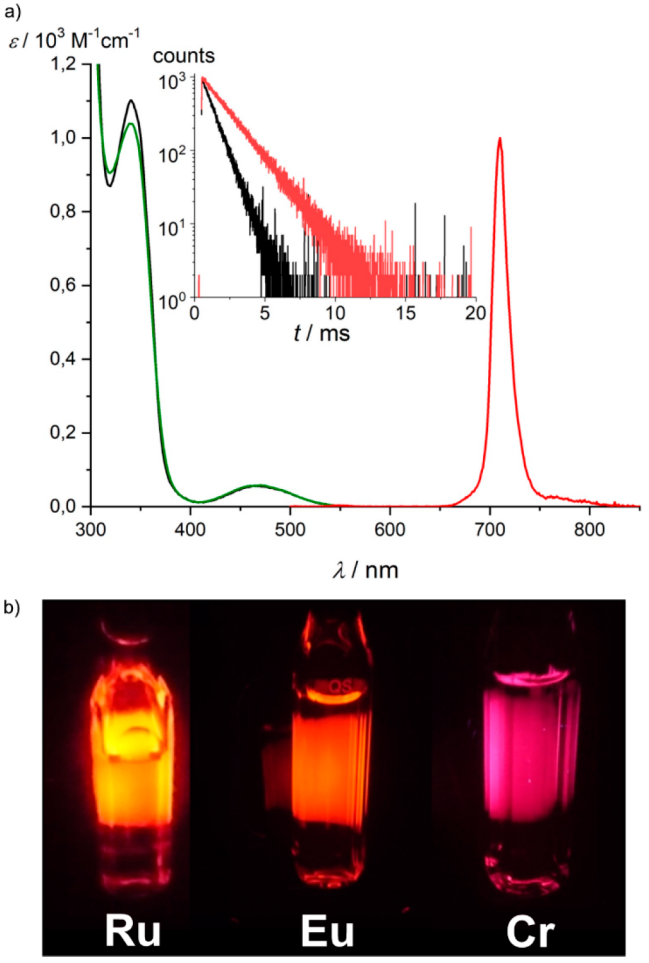

Figure 3. (a) UV/vis absorption spectrum (black), excitation spectrum (λ_{obs} = 709 nm, green), and emission spectrum (λ_{exc} = 462 nm, red) of $[Cr(bpmp)_2][OTf]_3$ in deaerated H_2O (0.1 M $HClO_4$) at room temperature; the inset shows the emission decay curves of $[Cr(bpmp)_2][OTf]_3$ in D_2O (0.1 M $DClO_4$) deaerated (red) and saturated with O_2 (black). b) Photographs of the red/orange emitters $[Ru(bpy)_3]^{2+}$, $[Eu(H_2O)(OTf)_2(tpy)_2]^+$, and the deep red emitter $[Cr(bpmp)_2]^{3+}$ in H_2O under irradiation with λ_{exc} = 340 nm.

deep red emission with CIE coordinates of x = 0.7326 and y = 0.2674 at the utmost corner of the CIE 1931 diagram (Figure 3b and Figure S22).[94]

The excitation spectrum (λ_{obs} = 709 nm) closely follows the absorption spectrum in the region of 300−600 nm. This confirms that the emission arises from the $[Cr(bpmp)_2]^{3+}$ chromophore. Furthermore, higher energy ^{4}LMCT states around 350 nm efficiently evolve to the luminescent state as well bypassing further loss channels (Figure 3a).

Gratifyingly, this emission band is higher in energy than that of $[Cr(ddpd)_2]^{3+}$ [53] by 1200 cm^{-1}, in agreement with the predicted trend of the CASSCF-NEVPT2 calculations (Figure 1). The experimentally determined excited state energies (lowest excited quartet and doublet states) reflect the quantum chemically predicted trends and confirm the validity of our screening strategy. The most important aspect is the red emission of $[Cr(bpmp)_2]^{3+}$ which is readily detected with conventional detectors. Although only a fraction of the sharp emission band tails into the visible red region (Figure 3a), the red emission under illumination in solution can even be observed by the naked eye (Figure 3b).

Upon cooling, the emission band sharpens further with a FWHM = 230 cm^{-1} at 130 K in frozen butyronitrile solution. Fine structure appears at the lower energy side of the emission band at lower temperature. The pattern can be fitted by five Voigt functions centered at 14140, 14017, 13788, 13483, and 13099 cm^{-1} (Figure S23). At lower temperature, the intensity of the three lower energy bands increases relative to the prominent 709 nm band at room temperature. This behavior is similar to that of $[Cr(ddpd)_2]^{3+}$ describing a Boltzmann distribution between two equilibrating emissive states.[53,55] The higher energy state is more emissive, that is, less prone to thermally activated nonradiative decay. This is confirmed by the luminescence spectra of a KBr pellet of $[Cr(bpmp)_2][BF_4]_3$ cooled to 10 K. Below ca. 130 K the low-energy emission (719.5 nm; 13900 cm^{-1}) dramatically increases in intensity, suggesting less efficient nonradiative decay pathways for this state at low temperature (Figure 4). Concomitantly, the high-energy

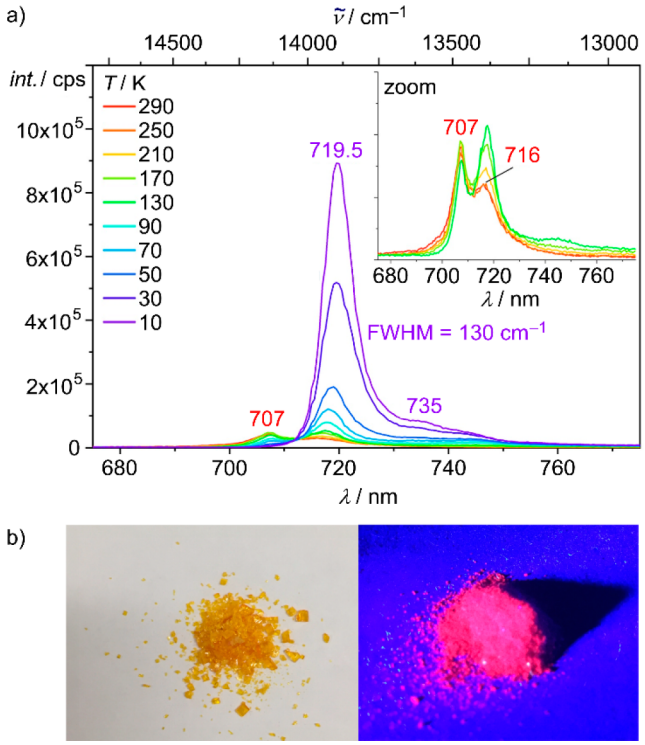

Figure 4. (a) Temperature-dependent luminescence spectra of $[Cr(bpmp)_2][BF_4]_3$ in a KBr matrix recorded between 10 K (purple) and 290 K (red) with λ_{exc} = 355 nm. The inset shows the spectra between 130 and 290 K. (b) Photographs of crystalline $[Cr(bpmp)_2][OTf]_3$ under ambient light and under irradiation with λ_{exc} = 340 nm.

emission (709 nm; 14105 cm^{-1}) vanishes. The energy difference is in the range predicted by the CASSCF(7,12)-NEVPT2 calculations for the two lowest doublet states (ΔE_{exp} = 245 cm^{-1}; ΔE_{CASSCF} = 154 cm^{-1}). The thermally activated nonradiative decay could be enabled by a surface crossing with the ground state, similar to the effects observed for $[Cr(tpe)_2]^{3+}$.[65] For this path to be operative, the lowest emissive state should be distorted relative to the ground state. This fits to a slightly distorted microstate of $^2T_1$ parentage which has been predicted by CASSCF(7,12)-NEVPT2 as the lowest doublet state. The presence of a vibrational fine structure of the low energy band confirms the distortion of this excited doublet state. Tentatively,

https://doi.org/10.1021/jacs.1c05971
J. Am. Chem. Soc. 2021, 143, 11843−11855

the vibrational progression of ca. 290 cm^{-1} could correspond to a Cr−N vibration (in the *xy*-plane) of the ground state according to the DFT calculations (308 cm^{-1}, scaled by 0.98:302 cm^{-1}; Figure S24). For $[Cr(NH_3)_6]^{3+}$, vibrations of odd symmetry $\delta(T_{1u}$, N−Cr−N) and $\nu(T_{1u}$, Cr−N) have been found at 267 and 458 cm^{-1}, respectively.[95]

The much higher integrated emission intensity upon cooling a sample of $[Cr(bpmp)_2][BF_4]_3$ in a KBr pellet from 290 to 10 K parallels an increase of the average photoluminescence lifetime from 38.0 to 1900 μs, respectively (Figure S25 and Table S8). The observed temperature dependence supports the model of reduced thermally available nonradiative decay pathways below ca. 130 K.

The photoluminescence quantum yield of $[Cr(bpmp)_2][OTf]_3$ reaches 12.3% at room temperature in deaerated H_2O solution (Table 1). This is similar to the quantum yield of the NIR emissive molecular ruby $[Cr(ddpd)_2]^{3+}$ and larger by several orders of magnitude compared to other reported chromium(III) emitters with emission in the red spectral region.[49] In pure and dry CH_3CN as well as in phosphate-buffered saline (PBS) buffer (0.1 M) the quantum yield drops below 2%, likely due to the deprotonation of the coordinated bpmp ligand in the ground state. Preventing CH_2 bridge deprotonation by adding $HClO_4$ increases the quantum yield to 15.8%. In the deuterated environments CD_3CN ($DClO_4$) and D_2O ($DClO_4$) the quantum yields increase to record numbers of 15.5% and 19.6%, respectively (Table 1). Other salts of $[Cr(bpmp)_2]^{3+}$ (ClO_4^-, PF_6^-, BF_4^-) show a similar behavior under acidic conditions (Table S9). The PF_6^- salt even reaches a quantum yield of 20% in $D_2O/DClO_4$ solution (Table S9). The acid/base chemistry and consequently the luminescence depend on the counterion in neutral to basic environments (Table S9).

Table 1. Quantum Yields Φ and Luminescence Lifetimes τ of $[Cr(bpmp)_2][OTf]_3$ and $[Cr([D_2]\text{-bpmp})_2][OTf]_3$ in Various Environments at Room Temperature (λ_{exc} = 462 nm)

solvent	acid[a]	O_2[c]	Φ (%)	τ (μs)
		$[Cr(bpmp)_2]^{3+}$		
H_2O		−	12.3	1360
H_2O	$HClO_4$	−	15.8	1550
H_2O	$HClO_4$	+	9.8	880
D_2O	$DClO_4$[b]	−	19.6	1800
D_2O	$DClO_4$[b]	+	9.8	840
CH_3CN		−	0.8	840
CH_3CN	$HClO_4$	−	11.4	1290
CH_3CN	$HClO_4$	+	4.6	390
CD_3CN	$DClO_4$[b]	−	15.5	1340
CD_3CN	$DClO_4$[b]	+	4.3	380
PBS (pH 6.6)		−	1.4	600
PBS (pH 6.4)		+	1.4	470
		$[Cr([D_2]\text{-bpmp})_2]^{3+}$		
D_2O	$DClO_4$	−	24.6	2500
D_2O	$DClO_4$	+	9.5	990

[a]Final $HClO_4$ ($DClO_4$) concentration c = 0.1 M. [b]Under these conditions, H → D exchange at the methylene bridge is expected. [c]"+" refers to atmospheric conditions and "−" to inert conditions.

In line with the above-mentioned acid/base chemistry, the CH acidic protons of the CH_2 bridges readily exchange with deuterium in D_2O (Figures S26 and S27). Replacement of CH by CD oscillators reduces the nonradiative excited state decay via multiphonon relaxation[54,57,96] involving the *aliphatic* CH/CD oscillators with Cr···H distances of 3.1−4.3 Å. Indeed, the quantum yield of $[Cr(bpmp)_2][OTf]_3$ increases from 15.8 to 19.6% by replacing $H_2O/HClO_4$ by $D_2O/DClO_4$ (Table 1). This gain results from the combined effect of the CH/CD replacement in the ligand methylene bridges and the OH/OD replacement in the aqueous solution. As the bridges rapidly exchange H/D in H_2O or D_2O, these first- and second-sphere isotope effects cannot be disentangled.

$[Cr(ddpd)_2]^{3+}$ with a lower emission energy has some spectral overlap with the third *aromatic* CH vibrational overtone ν^4_{CH} at ≈11493 cm^{-1} with a comparably high extinction coefficient.[54] Deuteration of $[Cr(ddpd)_2]^{3+}$ to $[Cr([D_x]\text{-ddpd})_2]^{3+}$ (>95% D at the pyridine α-positions which are closest to the metal center) increased the quantum yield to 30% in CD_3CN.[54] The spectral overlap integral of the sharp $[Cr(bpmp)_2]^{3+}$ emission band at 14124 cm^{-1} with overtones of *aromatic* CH oscillators is rather small as the accepting energy level derives from the fourth vibrational overtone ν^5_{CH} at ≈14065 cm^{-1}.[54] This high overtone possesses a very small extinction coefficient.[54] To ascertain whether a further boost of the quantum yield could be achieved by deuteration of aromatic ligand protons, the ligand $[D_2]$-bpmp with the pyridine's α-positions deuterated and its chromium complex $[Cr([D_2]\text{-bpmp})_2]^{3+}$ were synthesized as detailed in the Supporting Information (Figures S28−S37). This deuteration at the α-position increases the luminescence quantum yield from Φ = 19.6% to Φ = 24.6% in $D_2O/DClO_4$ (Table 1). Concomitantly, the lifetime increases from 1800 to 2500 μs (Table 1). This substantial increase in luminescence efficiency can be traced back to the comparison of spectral overlap of the relevant isotopologic C−(H/D) overtones with the doublet emission of chromium (Figures S38−S43). The fourth CH overtone (ν^5_{CH}) shows good spectral overlap (Figure S42), leading to a substantial nonradiative relaxation, while CD oscillators have a much smaller spectral overlap (Figure S43), in addition to the generally decreased oscillator strength compared to CH oscillators.

The photophysical properties of $[Cr(bpmp)_2]^{3+}$ and $[Cr([D_2]\text{-bpmp})_2]^{3+}$ outperform the record NIR photoluminescence data of the molecular ruby $[Cr(ddpd)_2]^{3+}$[54] and the standard red-orange emitter $[Ru(bpy)_3]^{2+}$ ($\Phi(CH_3CN)$ = 9.5%; $\tau(CH_3CN)$ = 1.1 μs; $\Phi(H_2O)$ = 6.3%; $\tau(H_2O)$ = 0.65 μs; Scheme 1).[97−99]

In the solid state, the details of the photoluminescence quantum yield and lifetime depend on the counterion. The quantum yield increases in the series BF_4^-, ClO_4^-, PF_6^-, and OTf^- (Φ = 0.5, 1.7, 2.0, and 7.1%) under aerated conditions. The luminescence decay was fitted mono-, bi-, or triexponentially and follows the same increasing trend with 36 μs, 89/230 μs (52:48), 530/250/110 μs (13:66:21), and 1100/520/190 μs (54:41:5), respectively. Clearly, the different packing and possible counterion association modify the solid state luminescence. Counterion effects on solid state and solution luminescence and photoreactivity have been reported previously for MLCT emitters,[100,101] yet a clear structure−activity relationship of counterion and luminescence in general, and spin-flip luminescence in particular,[102] is still elusive and more data are required.

The very long lifetime of the emissive state(s) allowed recording step-scan FT-IR spectra[44,65,103−105] after excitation of $[Cr(bpmp)_2][BF_4]_3$ in a KBr pellet with 355 nm excitation at 290 and 20 K (Figure 5a and Figures S44−S49). This high energy pulse likely populates allowed ^{4}LMCT states with

https://doi.org/10.1021/jacs.1c05971
J. Am. Chem. Soc. 2021, 143, 11843−11855

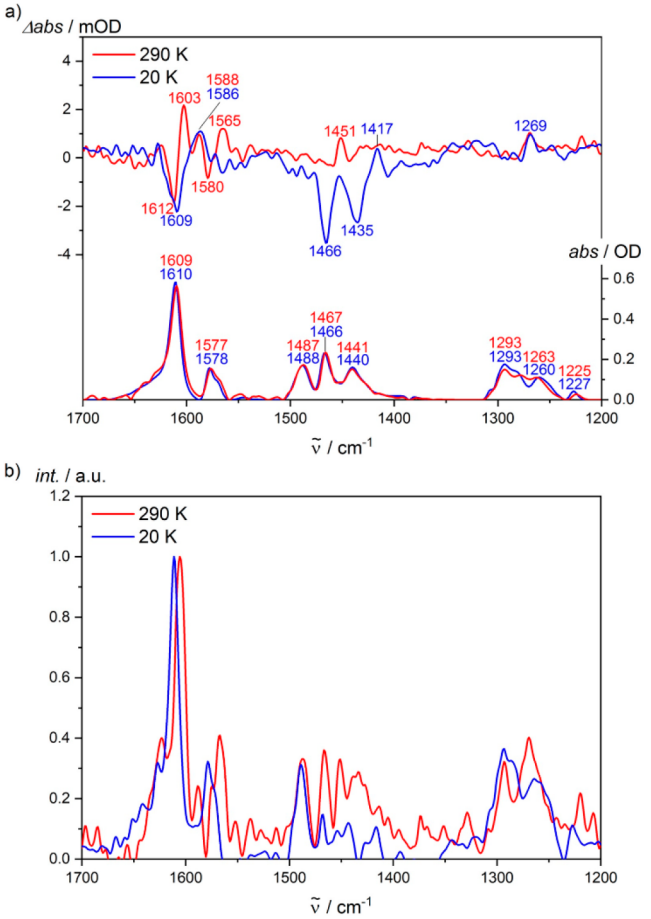

Figure 5. (a) Ground state (bottom) and step-scan FT-IR spectra (top, λ_{exc} = 355 nm; 0−1 μs) of $[Cr(bpmp)_2][BF_4]_3$ in a KBr pellet at 20 K (blue) and 290 K (red) and (b) excited state FT-IR spectra of $[Cr(bpmp)_2][BF_4]_3$ in a KBr pellet obtained from step-scan FT-IR spectra (λ_{exc} = 355 nm; 0−1 μs) (small contributions of 2% and 0.8% added to the respective ground state spectrum) at 20 K (blue) and 290 K (red). At 20 K, essentially the lowest doublet state is populated.

pyridine → t_{2g} CT character according to TD-DFT calculations (Figure 1 and Figure S21). The absorption and emission spectra are hardly affected by the matrix (solution, KBr pellet, thin film; Figures S50 and S51). The ground state FT-IR spectra are essentially superimposable at 290 and 20 K (Figure S44). On the other hand, the normalized excited state spectra show significant differences around 1600 cm^{-1}, 1550 cm^{-1}, and between 1400 and 1450 cm^{-1} at 290 and 20 K (Figure 5b). This is an indication for a temperature-dependent population of the contributing long-lived excited doublet states. With an estimated energy difference of the two lowest doublet microstates of $^2T_1$ and ^2E parentage of 245 cm^{-1} from the luminescence spectra (155 cm^{-1} from the CASSCF-NEVPT2 calculations), the derived Boltzmann population ratio amounts to 77:23 (CASSCF: 68:32) and 100:0 (CASSCF: 100:0) at 290 and 20 K, respectively. Consequently, only the lowest energy excited state is populated at 20 K. At 290 K, the rise and decay of the most prominent IR bands at 1612, 1603, 1588, and 1451 cm^{-1} were considered in a global fit to yield biexponential decays of 37 and 2.5 μs with contributions of 77% and 23%, respectively (Figure S48). This ratio matches the population ratio estimated from the luminescence energies. At 20 K, the higher doublet state is hardly populated. Indeed, the global fit of the IR bands yields a major time constant of 372 μs (96%) and a minor one of 13 μs (4%) (Figure S49). As thermal equilibration is not feasible at 20 K, the minor component might arise from the branching dynamics along the decay cascade after ^{4}LMCT excitation to the final excited $^2E/^2T_1$ states (Figure 1, purple arrows).

To experimentally probe the initial dynamics after excitation, subpicosecond transient absorption (TA) spectra of $[Cr(bpmp)_2][OTf]_3$ in CH_3CN ($HClO_4$) were recorded with excitation at 515 nm ($^4T_2$), 460 nm ($^4T_2$), and 350 nm (^{4}LMCT) (Figure 6 and Figures S52−S54). The TA spectra of

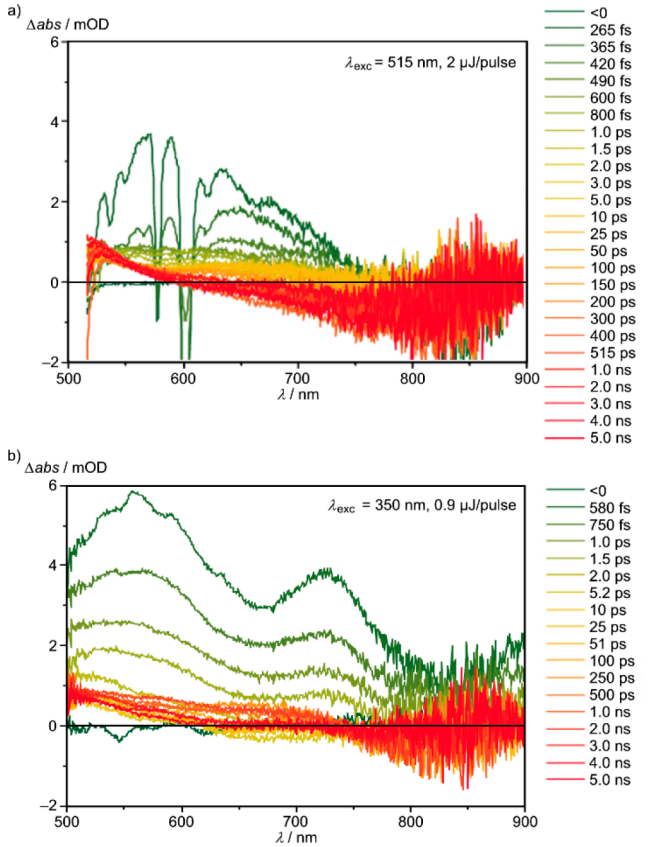

Figure 6. Transient absorption spectra of $[Cr(bpmp)_2][OTf]_3$ in CH_3CN ($HClO_4$) excited with femtosecond laser pulses (a) at 515 nm ($^4T_2$ states) and (b) at 350 nm (^{4}LMCT states).

the 515 and 460 nm excitation are very similar apart from the lower pump laser power at 460 nm, confirming that the same initial states are populated (Figure 6a and Figure S54). The TA spectra after $^4T_2$ excitation with 515 nm (Figure 6a) were fitted with three time constants $\tau^{515}{}_{1,2,3}$ of <200 fs, 300 ps, and a nondecaying component within the 8 ns time window, respectively. The fast decaying component $\tau^{515}{}_1$ is attributed to a coherent artifact necessary for the fit. The slow decaying component $\tau^{515}{}_3$ is straightforwardly assigned to the long-lived $^2E/^2T_1$ states. As the evolution-associated difference spectra (EADS) relating to τ_2 and τ_3 are similar lacking significant spectral shifts (Figure S52), they correspond to states of similar nature. A kinetic model assigns $\tau^{515}{}_2$ = 300 ps to internal conversion (IC) and vibrational cooling (VC) within doublet states $k(IC_1+VC_1)$ (Figure 1) while intersystem crossing (ISC) is faster than the instrument's time resolution ($\tau^{515}{}_1(ISC_1)$ < 200 fs). The combined ISC_1, IC_1, and VC_1 processes are slower than observed for $[Cr(ddpd)_2]^{3+}$ with 3.5 ps,[56] $Cr(acac)_3$ with 1.1 ps

https://doi.org/10.1021/jacs.1c05971
J. Am. Chem. Soc. 2021, 143, 11843−11855

(τ(ISC) < 100 fs),[107] Cr(*t*Buacac)$_3$ with 1.6 ps,[108] and $[Cr(CN)_6]^{3-}$ in a Cr^{III}–V^{III} Prussian blue analogue with τ(ISC) = 250 fs and τ(VC) = 1.1 ps[109] after $^4T_2$ excitation, while ISC occurs in the ultrafast time regime within hundreds of femtoseconds. The density of doublet states in the $^4T_2$ energy region and spin–orbit coupling (SOC) determine the ISC rates. For Cr(acac)$_3$ with nearly isoenergetic $^4T_2$ and $^2E/^2T_1$ states, SOC matrix elements between the $^4T_2$ and the $^2E/^2T_1$ states at geometries close to potential energy crossing points were calculated as 21–371 cm^{-1} (at the SOC-CASSCF(3,5) level of theory).[106] SOC-CASSCF(7,12)-NEVPT2 calculations for $[Cr(bpmp)_2]^{3+}$ (in the ground state geometry) deliver SOCs between the lowest quartet state $^4T_2(1)$ and the lowest doublet states derived from ^2E and $^2T_1$ states ranging from 6 to 97 cm^{-1} accounting for an ISC pathway from $^4T_2(1)$ to the doublet states, in particular the $^2E(1)$ state (Table S4). These values closely match those obtained for $[Cr(ddpd)_2]^{3+}$ (Table S4). The different SOCs for states of ^2E and $^2T_1$ parentage might account for the population of both $^2E(1)$ and states $^2T_1(1)$ at very low temperature without equilibration of these states.

The TA spectra after ^{4}LMCT excitation at 350 nm excitation (~Figure 6b) were fitted with three time constants $\tau^{350}{}_{1,2,3}$ of 540 fs, 75 ps, and a nondecaying component within the 8 ns time window. Again, $\tau^{350}{}_3$ is assigned to the lifetime of the $^2E/^2T_1$ states. The first EADS comprises a broad excited state absorption (ESA), with peaks at 560 and 740 nm (Figure S53). This decays in 540 fs to yield the second EADS, which shows an ESA at 525 nm. This evolves in 75 ps to the final EADS with a broad ESA, spanning 500–750 nm. The ESAs of the second and third EADS are rather similar and distinct from the first EADS. A plausible kinetic model assigns the fast component $\tau^{350}{}_1$ to ISC (and possibly electron redistribution) from ^{4}LMCT states to the metal-centered or charge-transfer doublet manifold [Figure 1; $\tau(ISC_2)$ = 540 fs] and the picosecond component $\tau^{350}{}_2$ to IC and VC within the doublets (Figure 1; $\tau(IC_2{+}VC_2)$ = 75 ps). ^{4}LMCT excitation of Cr(acac)$_3$ yielded a process of ~50 fs which had been tentatively assigned to the ^{4}LMCT to ^2E population transfer.[107] With these assignments, the conversion from the LMCT to the ligand field manifold is ~10 times slower in $[Cr(bpmp)_2]^{3+}$ than in Cr(acac)$_3$ which might be ascribed to a different density of (electronic and associated vibrational) doublet states in the respective CT energy regions and the very different ligand types.

Irrespective of the excitation energy and the decay pathway, the relaxed long-lived doublet state(s) of $[Cr(bpmp)_2]^{3+}$ are characterized by an ESA around 500–750 nm (Figure 6 and Figure S54), similar to the excited doublet states of $[Cr(ddpd)_2]^{3+}$ (530 nm)[56] and Cr(acac)$_3$ (510 nm).[108]

Singlet Oxygen Generation, Photoredox Chemistry, and Optical pH Sensing. The excited state reactivity of the long-lived doublet states of $[Cr(bpmp)_2][OTf]_3$ was probed by excited state quenching with oxygen in $H_2O/HClO_4$ and $CH_3CN/HClO_4$ (Table 1). In air-saturated solutions, the luminescence quantum yields were diminished by factors of 1.6 and 2.0, respectively. This is considerably less than observed for $[Cr(ddpd)_2][BF_4]_3$ with factors of 5.2 and 17, respectively.[53] The product of this reaction is singlet oxygen $^1O_2$ as confirmed by the observation of its characteristic emission at 1275 nm (Figure S55). Steady-state and time-resolved Stern–Volmer analyses yield Stern–Volmer constants $K_{SV} = 0.44 \times 10^4$ and 0.46×10^4 M^{-1}, respectively (Figures S56 and S57), demonstrating the dynamic character of the Dexter-type energy transfer quenching without significant static contributions.[110] With τ = 1550 μs, the bimolecular quenching rate constant k_q amounts to 0.29×10^7 M^{-1} s^{-1}. The longer lifetime of $[Cr(bpmp)_2]^{3+}$ and the lower K_{SV} as compared to those of $[Cr(ddpd)_2]^{3+}$[53] yield a lower bimolecular quenching rate constant k_q. The Stern–Volmer constants of the tetrafluoroborate salt are even lower than those of the triflate with $K_{SV} = 0.35 \times 10^4$ and 0.36×10^4 M^{-1} (intensity and lifetime based; Figures S58 and S59). The quenching rate constant was calculated to $k_q = 0.25 \times 10^7$ M^{-1} s^{-1} (τ = 1400 μs). The singlet oxygen quantum yields of $[Cr(bpmp)_2][X]_3$ were determined by using the comparative method as 55, 44, and 39% in DMF/$HClO_4$ for X^- = OTf^-, PF_6^-, and BF_4^-, respectively. These values are smaller than those of $[Cr(ddpd)_2][BF_4]_3$ in DMF (61%)[56] and in DMF/$HClO_4$ (86%) (Figure S55 and Table S5).

Although the driving force for energy transfer to oxygen is larger for $[Cr(bpmp)_2]^{3+}$ by 1200 cm^{-1} than for $[Cr(ddpd)_2]^{3+}$, and although the chromium center is somewhat less shielded by the CH_2 bridges than by the larger NCH_3 bridges of the ligands, $[Cr(bpmp)_2]^{3+}$ is less sensitive to oxygen than $[Cr(ddpd)_2]^{3+}$. A hypothesis for explaining this surprising result might be the dynamic association with the X^- counterions at the C–H acidic methylene bridges of the ligands, fully analogous to the coordination of triflates and tetrafluoroborates in the solid state structure (Figure 2b and Figure S14). Possibly, this dynamic coordination of the anions to the bridges in solution shields the chromium center in $[Cr(bpmp)_2]^{3+}$ from successful quenching encounters with O_2 more efficiently than the larger NCH_3 bridges which cannot hydrogen-bond to counterions. Consequently, the pockets spanned by the tridentate ligands are on average more often filled by counterions in the bpmp complex. These results might pave the way to successfully design *oxygen-insensitive* and *anion-sensitive* spin-flip emitters in the future.

Apart from excited state energy transfer, photoinduced single electron transfer could occur from suitable substrates to the excited chromium(III) complex. The favorable redox and excited state properties suggest the use of $[Cr(bpmp)_2][OTf]_3$ as photoredox sensitizer. The excited state is strongly oxidizing (0.94 V vs ferrocene), slightly more oxidizing than $*[Cr(tpe)_2]^{3+}/[Cr(tpe)_2]^{2+}$ (0.87 V vs ferrocene)[65] and significantly more oxidizing than $*[Ru(bpy)_3]^{2+}/[Ru(bpy)_3]^{+}$ (0.41 V vs ferrocene) or classical ground state ruthenium(III) oxidants $[Ru(bpy)_3]^{3+}$ (0.84 V vs ferrocene) and $[Ru(phen)_3]^{3+}$ (0.87 V vs ferrocene).[111]

In fact, azulene ($E_{1/2}$ = 0.50 V vs ferrocene)[112] quenches the emission of $[Cr(bpmp)_2]^{3+}$ ($K_{SV} = 3.73 \times 10^4$ M^{-1}; $k_q = 4.4 \times 10^7$ M^{-1} s^{-1} in CH_3CN; τ = 840 μs; Figure S60) slightly more efficiently than that of $[Cr(tpe)_2]^{3+}$ ($K_{SV} = 4.17 \times 10^4$ M^{-1}; $k_q = 1.4 \times 10^7$ M^{-1} s^{-1}). The larger driving force and hence a smaller activation barrier for the electron transfer between $*[Cr(bpmp)_2]^{3+}$ and azulene might account for this small difference. The small quenching rate constants of both complexes might be associated with a weak electronic coupling in the collision complex as a result of the metal-localized excited state and the formation of contact ion pairs with the counterions shielding the sensitizer. Unfortunately, photoinduced oxidation of amines as useful redox partners is not feasible due to the deprotonation of the CH_2 bridge of the coordinated ligand by amines already in the ground state (Figure 7). Yet, this intriguing feature can be turned into an advantage for sensing applications.

The reversible ground state acid/base chemistry forms dearomatized/rearomatized pyridine ligands.[113] Deprotonation at the methylene bridge leads to a coordinated nitrogen donor

https://doi.org/10.1021/jacs.1c05971
J. Am. Chem. Soc. 2021, 143, 11843–11855

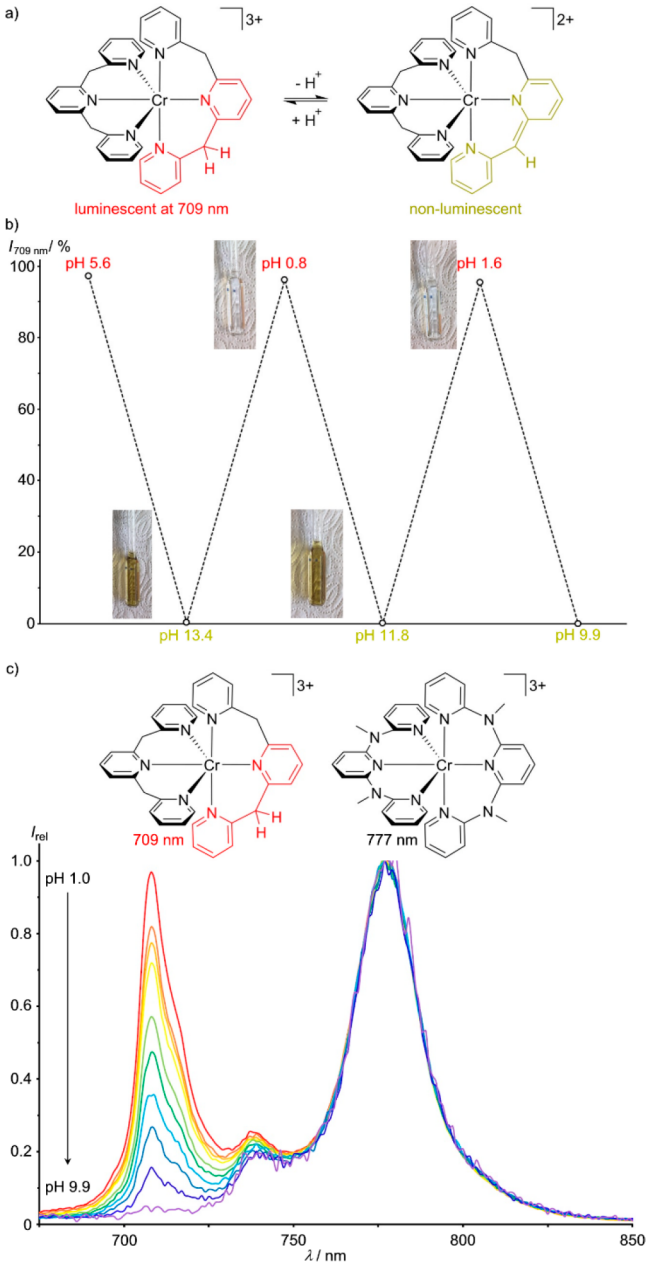

Figure 7. (a) Deprotonation/reprotonation equilibrium of an aqueous solution of $[Cr(bpmp)_2]^{3+}$ with concomitant dearomatization/rearomatization of a pyridine donor. (b) Intensity of the emission band at 709 nm during deprotonation/reprotonation cycles with NaOH and HOTf (λ_{exc} = 466 nm). (c) Normalized pH-dependent emission spectra of a mixture of $[Cr(bpmp)_2]^{3+}$ and $[Cr(ddpd)_2]^{3+}$ (molar fraction 25:2; λ_{exc} = 452 nm) in H_2O under ambient conditions. Note that dissolved O_2 reduces the quantum yield of both complexes especially at higher pH, and the nonemissive deprotonated complexes absorb strongly at the excitation wavelength. Both effects result in a poorer S/N ratio at high pH.

atom with enamide character dramatically changing the donor properties (Figure 7a). As a result, the luminescence of $[Cr(bpmp)_2]^{3+}$ at 709 nm is completely quenched at higher pH and reinstalled at lower pH (Figure 7b). As the emission of $[Cr(ddpd)_2]^{3+}$ at 777 nm is pH-insensitive, the combination of these two emitters gives a ratiometric optical pH sensor operating in the red to near-infrared spectral region with single-wavelength excitation in the blue (Figure 7c). The sharp emission bands of both complexes in the red/near-IR spectral region and the excitation with blue light would even allow combination with further luminophores utilizing the visible part of the spectral region.[60] Consequently, this luminophore combination will be further developed towards multicolor multianalyte optical probes in the future.[60]

CONCLUSIONS

On the basis of high-level computer-aided design, we developed the first molecular highly luminescent chromium(III) complex emitting in the red spectral region. After excitation of the $[Cr(bpmp)_2]^{3+}$ luminophore, ultrafast and efficient population transfer by intersystem crossing and vibrational cooling to the long-lived doublet states of $*[Cr(bpmp)_2]^{3+}$ occurs. These doublet states emit in the deep red spectral region with photoluminescence quantum yields up to 20% and excited state lifetimes up to 1800 μs. Deuteration of the α-positions of the terminal pyridines increases the quantum yield to 25% and the lifetime to 2500 μs. The key photophysical properties of the purely red-emissive molecular ruby $[Cr(bpmp)_2]^{3+}$ (emission color, photoluminescence quantum yield, excited state lifetime, and excited state redox potential) outperform those of the classical ruthenium(II) sensitizers and the often-used europium(III)-based red-emissive complexes. Furthermore, the reversible ground state (de)protonation of $[Cr(bpmp)_2]^{3+}$ coupled with an off/on luminescence enables ratiometric optical pH sensing. Future work will further exploit this novel red emitter with an earth-abundant chromium center in bioimaging, multicolor sensing (e.g., pH, O_2, and anions), photocatalysis, molecular upconversion,[61,114] and circularly polarized luminescence.[63,64,115−117]

ASSOCIATED CONTENT

Supporting Information

The Supporting Information is available free of charge at https://pubs.acs.org/doi/10.1021/jacs.1c05971.

Details of quantum chemical calculations, synthetic procedures, analytical and spectroscopic data of $Cr(bpmp)Cl_3$, $Cr(bpmp)Br_3$, $Cr(bpmp)(OTf)_3$, $[Cr(bpmp)_2][OTf]_3$, $[Cr(bpmp)_2][BF_4]_3$, $[Cr(bpmp)_2][PF_6]_3$, $[D_2]$-bpmp, $Cr([D_2]\text{-bpmp})Cl_3$, $Cr([D_2]\text{-bpmp})(OTf)_3$, and $[Cr([D_2]\text{-bpmp})_2][OTf]_3$ (PDF)

Video S1 (MP4)

Video S2 (MP4)

Accession Codes

CCDC 1989536−1989537 and 2083757 contain the supplementary crystallographic data for this paper. These data can be obtained free of charge via www.ccdc.cam.ac.uk/data_request/cif, or by emailing data_request@ccdc.cam.ac.uk, or by contacting The Cambridge Crystallographic Data Centre, 12 Union Road, Cambridge CB2 1EZ, UK; fax: +44 1223 336033.

AUTHOR INFORMATION

Corresponding Authors

Katja Heinze − *Department of Chemistry, Johannes Gutenberg University of Mainz, 55128 Mainz, Germany;* orcid.org/0000-0003-1483-4156; Email: katja.heinze@uni-mainz.de

Ute Resch-Genger − *Division Biophotonics, Federal Institute for Materials Research and Testing (BAM), 12489 Berlin, Germany;* orcid.org/0000-0002-0944-1115; Email: ute.resch@bam.de

Michael Seitz − *Institute of Inorganic Chemistry, University of Tübingen, 72076 Tübingen, Germany;* orcid.org/0000-0002-9313-2779; Email: michael.seitz@uni-tuebingen.de

Authors

Florian Reichenauer − *Department of Chemistry, Johannes Gutenberg University of Mainz, 55128 Mainz, Germany*

Cui Wang − *Division Biophotonics, Federal Institute for Materials Research and Testing (BAM), 12489 Berlin, Germany; Institut für Chemie und Biochemie, Freie Universität Berlin, 14195 Berlin, Germany*

Christoph Förster − *Department of Chemistry, Johannes Gutenberg University of Mainz, 55128 Mainz, Germany*

Pit Boden − *Department of Chemistry and Research Center Optimas, University Kaiserslautern, 67663 Kaiserslautern, Germany*

Naz Ugur − *Max Planck Institute for Polymer Research, 55128 Mainz, Germany*

Ricardo Báez-Cruz − *Max Planck Institute for Polymer Research, 55128 Mainz, Germany*

Jens Kalmbach − *Institute of Inorganic Chemistry, University of Tübingen, 72076 Tübingen, Germany*

Luca M. Carrella − *Department of Chemistry, Johannes Gutenberg University of Mainz, 55128 Mainz, Germany*

Eva Rentschler − *Department of Chemistry, Johannes Gutenberg University of Mainz, 55128 Mainz, Germany;* orcid.org/0000-0003-1431-3641

Charusheela Ramanan − *Max Planck Institute for Polymer Research, 55128 Mainz, Germany*

Gereon Niedner-Schatteburg − *Department of Chemistry and Research Center Optimas, University Kaiserslautern, 67663 Kaiserslautern, Germany;* orcid.org/0000-0001-7240-6673

Markus Gerhards − *Department of Chemistry and Research Center Optimas, University Kaiserslautern, 67663 Kaiserslautern, Germany;* orcid.org/0000-0002-8748-2940

Complete contact information is available at: https://pubs.acs.org/10.1021/jacs.1c05971

Notes

The authors declare no competing financial interest.

During manuscript finalization, Prof. Markus Gerhards unexpectedly passed away on Dec 28th 2020.

■ ACKNOWLEDGMENTS

Financial support from the Deutsche Forschungsgemeinschaft [DFG, Priority Program SPP 2102 "Light-controlled reactivity of metal complexes" (GE 961/10-1, HE 2778/15-1, SE 1448/8-1] and RE 1203/23-1 is gratefully acknowledged. Parts of this research were conducted by using the supercomputer Mogon and advisory services offered by Johannes Gutenberg University Mainz (www.hpc.uni-mainz.de), which is a member of the AHRP and the Gauss Alliance e.V., and the supercomputer Elwetritsch and advisory services offered by the TU Kaiserslautern (https://elwe.rhrk.uni-kl.de), which is a member of the AHRP. We thank Marius Bauer and Leander Geske for assistance with photography and IR spectroscopy, respectively.

■ REFERENCES

(1) Baldo, M. A.; Thompson, M. E.; Forrest, S. R. High-Efficiency Fluorescent Organic Light-Emitting Devices using a Phosphorescent Sensitizer. *Nature* **2000**, *403*, 750−753.

(2) Li, A.; Turro, C.; Kodanko, J. J. Ru(II) Polypyridyl Complexes Derived from Tetradentate Ancillary Ligands for Effective Photocaging. *Acc. Chem. Res.* **2018**, *51*, 1415−1421.

(3) Mari, C.; Pierroz, V.; Ferrari, S.; Gasser, G. Combination of Ru(II) Complexes and Light: New Frontiers in Cancer Therapy. *Chem. Sci.* **2015**, *6*, 2660−2686.

(4) Hagfeldt, A.; Grätzel, M. Molecular Photovoltaics. *Acc. Chem. Res.* **2000**, *33*, 269−277.

(5) Yoon, T. P.; Ischay, M. A.; Du, J. N. Visible Light Photocatalysis as a Greener Approach to Photochemical Synthesis. *Nat. Chem.* **2010**, *2*, 527−532.

(6) Marzo, L.; Pagire, S. K.; Reiser, O.; König, B. Visible-light photocatalysis: does it make a difference in organic synthesis? *Angew. Chem., Int. Ed.* **2018**, *57*, 10034−10072.

(7) Romero, N. A.; Nicewicz, D. A. Organic photoredox catalysis. *Chem. Rev.* **2016**, *116*, 10075−10166.

(8) Skubi, K. L.; Blum, T. R.; Yoon, T. P. Dual Catalysis Strategies in Photochemical Synthesis. *Chem. Rev.* **2016**, *116*, 10035−10074.

(9) Shaw, M. H.; Twilton, J.; MacMillan, D. W. Photoredox catalysis in organic chemistry. *J. Org. Chem.* **2016**, *81*, 6898−926.

(10) Narayanam, J. M.; Stephenson, C. R. Visible light photoredox catalysis. Applications in organic synthesis. *Chem. Soc. Rev.* **2011**, *40*, 102−113.

(11) Herr, P.; Glaser, F.; Büldt, L. A.; Larsen, C. B.; Wenger, O. S. Long-Lived, Strongly Emissive, and Highly Reducing Excited States in Mo(0) Complexes with Chelating Isocyanides. *J. Am. Chem. Soc.* **2019**, *141*, 14394−14402.

(12) Büldt, L. A.; Wenger, O. S. Chromium(0), Molybdenum(0), and Tungsten(0) Isocyanide Complexes as Luminophores and Photosensitizers with Long-Lived Excited States. *Angew. Chem., Int. Ed.* **2017**, *56*, 5676−5682.

(13) Büldt, L. A.; Guo, X.; Prescimone, A.; Wenger, O. S. A Molybdenum(0) Isocyanide Analogue of $Ru(2,2\text{-Bipyridine})_3^{2+}$: A Strong Reductant for Photoredox Catalysis. *Angew. Chem., Int. Ed.* **2016**, *55*, 11247−11250.

(14) Yam, V. W.; Wong, K. M.-C. Luminescent metal complexes of d^6, d^8 and d^{10} transition metal centres. *Chem. Commun.* **2011**, *47*, 11579−11592.

(15) Hamze, R.; Peltier, J. L.; Sylvinson, D.; Jung, M.; Cardenas, J.; Haiges, R.; Soleilhavoup, M.; Jazzar, R.; Djurovich, P. I.; Bertrand, G.; Thompson, M. E. Eliminating Nonradiative Decay in Cu(I) Emitters: > 99% Quantum Efficiency and Microsecond Lifetime. *Science* **2019**, *363*, 601−606.

(16) Gernert, M.; Müller, U.; Haehnel, M.; Pflaum, J.; Steffen, A. A Cyclic Alkyl(amino)carbene as Two-Atom π-Chromophore Leading to the First Phosphorescent Linear Cu^I Complexes. *Chem. - Eur. J.* **2017**, *23*, 2206−2216.

(17) Di, D. W.; Romanov, A. S.; Yang, L.; Richter, J. M.; Rivett, J. P. H.; Jones, S.; Thomas, T. H.; Abdi Jalebi, M.; Friend, R. H.; Linnolahti, M.; Bochmann, M.; Credgington, D. High-Performance Light-Emitting Diodes based on Carbene-Metal-Amides. *Science* **2017**, *356*, 159−163.

(18) Hossain, A.; Bhattacharyya, A.; Reiser, O. Copper's Rapid Ascent in Visible-Light Photoredox Catalysis. *Science* **2019**, *364*, eaav9713.

(19) Hernandez-Perez, A. C.; Collins, S. K. Heteroleptic Cu-Based Sensitizers in Photoredox Catalysis. *Acc. Chem. Res.* **2016**, *49*, 1557−1565.

(20) Housecroft, C. E.; Constable, E. C. The emergence of copper(i)-based dye sensitized solar cells. *Chem. Soc. Rev.* **2015**, *44*, 8386−8398.

(21) Yersin, H.; Rausch, A. F.; Czerwieniec, R.; Hofbeck, T.; Fischer, T. The triplet state of organo-transition metal compounds. Triplet harvesting and singlet harvesting for efficient OLEDs. *Coord. Chem. Rev.* **2011**, *255*, 2622−2652.

(22) Zhang, Y.; Schulz, M.; Wächtler, M.; Karnahl, M.; Dietzek, B. Heteroleptic diimine−diphosphine Cu(I) complexes as an alternative towards noble-metal based photosensitizers: Design strategies, photophysical properties and perspective applications. *Coord. Chem. Rev.* **2018**, *356*, 127−146.

(23) Förster, C.; Heinze, K. Photophysics and photochemistry with Earth-abundant metals - fundamentals and concepts. *Chem. Soc. Rev.* **2020**, *49*, 1057−1070.
(24) Hockin, B. M.; Li, C.; Robertson, N.; Zysman-Colman, E. Photoredox catalysts based on earth-abundant metal complexes. *Catal. Sci. Technol.* **2019**, *9*, 889−915.
(25) Wenger, O. S. Photoactive Complexes with Earth-Abundant Metals. *J. Am. Chem. Soc.* **2018**, *140*, 13522−13533.
(26) Otto, S.; Dorn, M.; Förster, C.; Bauer, M.; Seitz, M.; Heinze, K. Understanding and Exploiting Long-lived Near-infrared Emission of a Molecular Ruby. *Coord. Chem. Rev.* **2018**, *359*, 102−111.
(27) Bizzarri, C.; Spuling, E.; Knoll, D. M.; Volz, D.; Bräse, S. Sustainable metal complexes for organic light-emitting diodes (OLEDs). *Coord. Chem. Rev.* **2018**, *373*, 49−82.
(28) Larsen, C. B.; Wenger, O. S. Photoredox Catalysis with Metal Complexes Made from Earth-Abundant Elements. *Chem. - Eur. J.* **2018**, *24*, 2039−2058.
(29) Bozic-Weber, B.; Constable, E. C.; Housecroft, C. E. Light harvesting with Earth abundant d-block metals: development of sensitizers in dye-sensitized solar cells (DSCs). *Coord. Chem. Rev.* **2013**, *257*, 3089−3106.
(30) Barbieri, A.; Accorsi, G.; Armaroli, N. Luminescent complexes beyond the platinum group: the d^{10} avenue. *Chem. Commun.* **2008**, 2185−2193.
(31) Harlang, T. C. B.; Liu, Y. Z.; Gordivska, O.; Fredin, L. A.; Ponseca, C. S.; Huang, P.; Chabera, P.; Kjaer, K. S.; Mateos, H.; Uhlig, J.; Lomoth, R.; Wallenberg, R.; Styring, S.; Persson, P.; Sundström, V.; Wärnmark, K. Iron Sensitizer Converts Light to Electrons with 92% Yield. *Nat. Chem.* **2015**, *7*, 883−889.
(32) Chábera, P.; Kjaer, K. S.; Prakash, O.; Honarfar, A.; Liu, Y. Z.; Fredin, L. A.; Harlang, T. C. B.; Lidin, S.; Uhlig, J.; Sundström, V.; Lomoth, R.; Persson, P.; Wärnmark, K. Fe^{II} Hexa N-Heterocyclic Carbene Complex with a 528 ps Metal-to-Ligand Charge-Transfer Excited-State Lifetime. *J. Phys. Chem. Lett.* **2018**, *9*, 459−463.
(33) Büldt, L. A.; Guo, X.; Vogel, R.; Prescimone, A.; Wenger, O. S. A Tris(diisocyanide)chromium(0) Complex Is a Luminescent Analog of $Fe(2,2'\text{-Bipyridine})_3^{2+}$. *J. Am. Chem. Soc.* **2017**, *139*, 985−992.
(34) Stevenson, S. M.; Shores, M. P.; Ferreira, E. M. Photooxidizing Chromium Catalysts for Promoting Radical Cation Cycloadditions. *Angew. Chem., Int. Ed.* **2015**, *54*, 6506−6510.
(35) Higgins, R. F.; Fatur, S. M.; Shepard, S. G.; Stevenson, S. M.; Boston, D. J.; Ferreira, E. M.; Damrauer, N. H.; Rappé, A. K.; Shores, M. P. Uncovering the Roles of Oxygen in Cr(III) Photoredox Catalysis. *J. Am. Chem. Soc.* **2016**, *138*, 5451−5464.
(36) Stevenson, S. M.; Higgins, R. F.; Shores, M. P.; Ferreira, E. M. Chromium photocatalysis: accessing structural complements to Diels−Alder adducts with electron-deficient dienophiles. *Chem. Sci.* **2017**, *8*, 654−660.
(37) Zhang, Y.; Lee, T. S.; Favale, J. M.; Leary, D. C.; Petersen, J. L.; Scholes, G. D.; Castellano, F. N.; Milsmann, C. Delayed fluorescence from a zirconium (iv) photosensitizer with ligand-to-metal charge-transfer excited states. *Nat. Chem.* **2020**, *12*, 345−352.
(38) Kjær, K. S.; Kaul, N.; Prakash, O.; Chábera, P.; Rosemann, N. W.; Honarfar, A.; Gordivska, O.; Fredin, L. A.; Bergquist, K. E.; Häggström, L.; Ericsson, T.; Lindh, L.; Yartsev, A.; Styring, S.; Huang, P.; Uhlig, J.; Bendix, J.; Strand, D.; Sundström, V.; Persson, P.; Lomoth, R.; Wärnmark, K. Luminescence and Reactivity of a Charge-Transfer Excited Iron Complex with Nanosecond Lifetime. *Science* **2019**, *363*, 249−253.
(39) Chábera, P.; Lindh, L.; Rosemann, N. W.; Prakash, O.; Uhlig, J.; Yartsev, A.; Wärnmark, K.; Sundström, V.; Persson, P. *Coord. Chem. Rev.* **2021**, *426*, 213517.
(40) Pal, A. K.; Li, C. F.; Hanan, G. S.; Zysman-Colman, E. Blue-Emissive Cobalt(III) Complexes and Their Use in the Photocatalytic Trifluoromethylation of Polycyclic Aromatic Hydrocarbons. *Angew. Chem., Int. Ed.* **2018**, *57*, 8027−8031.
(41) Yam, V. W.; Chan, A. K.; Hong, E. Y. Charge-transfer processes in metal complexes enable luminescence and memory functions. *Nat. Rev. Chem.* **2020**, *4*, 528−541.
(42) Jamieson, M. A.; Serpone, N.; Hoffman, M. Z. Advances in the photochemistry and photophysics of chromium(III) polypyridyl complexes in fluid media. *Coord. Chem. Rev.* **1981**, *39*, 121−179.
(43) Kirk, A. D. Photochemistry and Photophysics of Chromium(III) Complexes. *Chem. Rev.* **1999**, *99*, 1607−1640.
(44) Dorn, M.; Kalmbach, J.; Boden, P.; Päpcke, A.; Gómez, S.; Förster, C.; Kuczelinis, F.; Carrella, L. M.; Büldt, L.; Bings, N.; Rentschler, E.; Lochbrunner, S.; González, L.; Gerhards, M.; Seitz, M.; Heinze, K. A vanadium(III) complex with blue and NIR-II spin-flip luminescence in solution. *J. Am. Chem. Soc.* **2020**, *142*, 7947−7955.
(45) Forster, L. S. Thermal relaxation in excited electronic states of d^3 and d^6 metal complexes. *Coord. Chem. Rev.* **2002**, *227*, 59−92.
(46) Forster, L. S. Intersystem crossing in transition metal complexes. *Coord. Chem. Rev.* **2006**, *250*, 2023−2033.
(47) Kane-Maguire, N. A. P. Photochemistry and Photophysics of Coordination Compounds: Chromium. *Top. Curr. Chem.* **2007**, *280*, 37−67.
(48) Balzani, V.; Ceroni, P.; Juris, A.. *Photochemistry and Photophysics*; Wiley-VCH: Weinheim, 2014; pp 216−219.
(49) Xiang, H.; Cheng, J.; Ma, X.; Zhou, X.; Chruma, J. J. Near-infrared phosphorescence: materials and applications. *Chem. Soc. Rev.* **2013**, *42*, 6128−6185.
(50) Jørgenson, C. K. Recent Progress in Ligand Field Theory. *Struct. Bonding (Berlin)* **1966**, *1*, 3−31.
(51) Breivogel, A.; Förster, C.; Heinze, K. A Heteroleptic Bis(tridentate)ruthenium(II) Polypyridine Complex with Improved Photophysical Properties and Integrated Functionalizability. *Inorg. Chem.* **2010**, *49*, 7052−7056.
(52) Förster, C.; Dorn, M.; Reuter, T.; Otto, S.; Davarci, G.; Reich, T.; Carrella, L.; Rentschler, E.; Heinze, K. Ddpd as Expanded Terpyridine: Dramatic Effects of Symmetry and Electronic Properties in First Row Transition Metal Complexes. *Inorganics* **2018**, *6*, 86.
(53) Otto, S.; Grabolle, M.; Förster, C.; Kreitner, C.; Resch-Genger, U.; Heinze, K. $[Cr(ddpd)_2]^{3+}$: A molecular, water-soluble, highly NIR-emissive ruby analogue. *Angew. Chem., Int. Ed.* **2015**, *54*, 11572−11576.
(54) Wang, C.; Otto, S.; Dorn, M.; Kreidt, E.; Lebon, J.; Sršan, L.; Di Martino-Fumo, P.; Gerhards, M.; Resch-Genger, U.; Seitz, M.; Heinze, K. Deuterated Molecular Ruby with Record Luminescence Quantum Yield. *Angew. Chem., Int. Ed.* **2018**, *57*, 1112−1116.
(55) Otto, S.; Scholz, N.; Behnke, T.; Resch-Genger, U.; Heinze, K. Thermo-Chromium: A Contactless Optical Molecular Thermometer. *Chem. - Eur. J.* **2017**, *23*, 12131−12135.
(56) Otto, S.; Nauth, A. M.; Ermilov, E.; Scholz, N.; Friedrich, A.; Resch-Genger, U.; Lochbrunner, S.; Opatz, T.; Heinze, T. Photo-Chromium: Sensitizer for Visible Light-Induced Oxidative C-H Bond Functionalization − Electron or Energy Transfer? *ChemPhotoChem.* **2017**, *1*, 344−349.
(57) Otto, S.; Förster, C.; Wang, C.; Resch-Genger, U.; Heinze, K. A strongly luminescent chromium(III) complex acid. *Chem. - Eur. J.* **2018**, *24*, 12555−12563.
(58) Otto, S.; Harris, J.; Heinze, K.; Reber, C. Molecular ruby under pressure. *Angew. Chem., Int. Ed.* **2018**, *57*, 11069−11073.
(59) Basu, U.; Otto, S.; Heinze, K.; Gasser, G. Biological Evaluation of the NIR-Emissive Ruby Analogue $[Cr(ddpd)_2][BF_4]_3$ as a Photodynamic Therapy Photosensitizer. *Eur. J. Inorg. Chem.* **2019**, *2019*, 37−41.
(60) Wang, C.; Otto, S.; Dorn, M.; Heinze, K.; Resch-Genger, U. Luminescent TOP Nanosensors for Simultaneously Measuring Temperature, Oxygen, and pH at a Single Excitation Wavelength. *Anal. Chem.* **2019**, *91*, 2337−2344.
(61) Kalmbach, J.; Wang, C.; You, Y.; Förster, C.; Schubert, H.; Heinze, K.; Resch-Genger, U.; Seitz, M. Near-IR to Near-IR Upconversion Luminescence in Molecular Chromium Ytterbium Salts. *Angew. Chem., Int. Ed.* **2020**, *59*, 18804−18808.
(62) Jiménez, J.-R.; Doistau, B.; Besnard, C.; Piguet, C. Versatile heteroleptic bis-terdentate Cr(III) chromophores displaying room temperature millisecond excited state lifetimes. *Chem. Commun.* **2018**, *54*, 13228−13231.

https://doi.org/10.1021/jacs.1c05971
J. Am. Chem. Soc. 2021, 143, 11843−11855

(63) Jiménez, J. R.; Doistau, B.; Cruz, C. M.; Besnard, C.; Cuerva, J. M.; Campaña, A. G.; Piguet, C. Chiral Molecular Ruby $[Cr(dqp)_2]^{3+}$ with Long-Lived Circularly Polarized Luminescence. *J. Am. Chem. Soc.* **2019**, *141*, 13244−13252.
(64) Dee, C.; Zinna, F.; Kitzmann, W. R.; Pescitelli, G.; Heinze, K.; Di Bari, L.; Seitz, M. Strong Circularly Polarized Luminescence of an Octahedral Chromium(III) Complex. *Chem. Commun.* **2019**, *55*, 13078−13081.
(65) Treiling, S.; Wang, C.; Förster, C.; Reichenauer, F.; Kalmbach, J.; Boden, P.; Harris, J. P.; Carrella, L. M.; Rentschler, E.; Resch-Genger, U.; Reber, C.; Seitz, M.; Gerhards, M.; Heinze, K. Luminescence and Light-driven Energy and Electron Transfer from an Exceptionally Long-lived Excited State of a Non-innocent Chromium(III) Complex. *Angew. Chem., Int. Ed.* **2019**, *58*, 18075−18085.
(66) Bünzli, J.-C. G.; Charbonniere, L. J.; Ziessel, R. F. Structural and photophysical properties of Ln^{III} complexes with 2,2'-bipyridine-6,6'-dicarboxylic acid: surprising formation of a H-bonded network of bimetallic entities. *J. Chem. Soc., Dalton Trans.* **2000**, 1917−1923.
(67) Wahsner, J.; Seitz, M. Nonradiative Deactivation of Lanthanoid Excited States by Inner-Sphere Carboxylates. *Inorg. Chem.* **2015**, *54*, 10841−10848.
(68) Bünzli, J.-C. G. Lanthanide Luminescence for Biomedical Analyses and Imaging. *Chem. Rev.* **2010**, *110*, 2729−2755.
(69) Heffern, M. C.; Matosziuk, L. M.; Meade, T. J. Lanthanide Probes for Bioresponsive Imaging. *Chem. Rev.* **2014**, *114*, 4496−4539.
(70) Amoroso, A. J.; Pope, S. J. A. Using lanthanide ions in molecular bioimaging. *Chem. Soc. Rev.* **2015**, *44*, 4723−4742.
(71) Degli Esposti, C.; Bizzocchi, L. Absorption and Emission Spectroscopy of a Lasing Material: Ruby. *J. Chem. Educ.* **2007**, *84*, 1316−1318.
(72) Dominiak-Dzik, G.; Ryba-Romanowski, W.; Grinberg, M.; Beregi, E.; Kovacs, L. Excited-state relaxation dynamics of Cr^{3+}in $YAl_3(BO_3)_4$. *J. Phys.: Condens. Matter* **2002**, *14*, 5229−5237.
(73) Malysa, B.; Meijerink, A.; Jüstel, T. Temperature dependent luminescence Cr^{3+}-doped $GdAl_3(BO_3)_4$ and $YAl_3(BO_3)_4$. *J. Lumin.* **2016**, *171*, 246−253.
(74) Harris, J. P.; Sonneville, C.; Villain, O.; Calas, G.; Reber, C. Analytical fitting of temperature-dependent spin-flip transitions in absorption spectra of Cr^{3+}-doped silicate glasses. *Chem. Phys. Lett.: X* **2019**, *2*, 100003.
(75) Sijbom, H.; Verstraete, R.; Joos, J. J.; Poelman, D.; Smet, P. F. K_2SiF_6:Mn^{4+} as a red phosphor for displays and warm-white LEDs: a review of properties and perspectives. *Opt. Mater. Express* **2017**, *7*, 3332−3365.
(76) Ballhausen, C. J. *Introduction to Ligand Field Theory*; McGraw-Hill: New York, 1962; p 222.
(77) Ballhausen, C. J. *Molecular Electronic Structures of Transition Metal Complexes*; McGraw-Hill: New York, 1979; p 1.
(78) Avram, N. M., Brik, M. G., Eds.; *Optical Properties of 3d-Ions in Crystals: Spectroscopy and Crystal Field Analysis*; Springer: 2013; p 62.
(79) Daniel, C. Photochemistry and photophysics of transition metal complexes: quantum chemistry. *Coord. Chem. Rev.* **2015**, *282*−*283*, 19−32.
(80) Sousa, C.; Alías, M.; Domingo, A.; de Graaf, C. Deactivation of Excited States in Transition-Metal Complexes: Insight from Computational Chemistry. *Chem. - Eur. J.* **2019**, *25*, 1152−1164.
(81) Reinen, D.; Atanasov, M.; Köhler, P.; Babel, D. Jahn−Teller coupling and the influence of strain in T_g and E_g ground and excited states − A ligand field and DFT study on halide $M^{III}X_6$ model complexes [M = Ti^{III}−Cu^{III}; X = F^-, Cl^-]. *Coord. Chem. Rev.* **2010**, *254*, 2703−2754.
(82) Escudero, D. Photodeactivation Channels of Transition Metal Complexes: A Computational Chemistry Perspective. In *Transition Metals in Coordination Environments*; Broclawik, E., Borowski, T., Radoń, M., Eds; Challenges and Advances in Computational Chemistry and Physics; Springer: Cham, 2019; Vol. *29*.
(83) Atanasov, M.; Ganyushin, D.; Sivalingam, K.; Neese, F. A Modern First-Principles View on Ligand Field Theory Through the Eyes of Correlated Multireference Wavefunctions. *Struct. Bonding (Berlin, Ger.)* **2011**, *143*, 149−220.
(84) Singh, S. K.; Eng, J.; Atanasov, M.; Neese, F. Covalency and chemical bonding in transition metal complexes: An ab initio based ligand field perspective. *Coord. Chem. Rev.* **2017**, *344*, 2−25.
(85) Lang, L.; Atanasov, M.; Neese, F. Improvement of Ab Initio Ligand Field Theory by Means of Multistate Perturbation Theory. *J. Phys. Chem. A* **2020**, *124*, 1025−1037.
(86) Pierloot, K.; Vancoillie, S. Relative energy of the high-($^5T_{2g}$) and low-($^1A_{1g}$) spin states of $Fe(H_2O)_6]^{2+}$, $Fe(NH_3)_6]^{2+}$, and $[Fe(bpy)_3]^{2+}$: CASPT2 versus density functional theory. *J. Chem. Phys.* **2006**, *125*, 124303.
(87) Pierloot, K. Transition metals compounds: Outstanding challenges for multiconfigurational methods. *Int. J. Quantum Chem.* **2011**, *111*, 3291−3301.
(88) Dyker, G.; Muth, O. Synthesis of Methylene- and Methine-Bridged Oligopyridines. *Eur. J. Org. Chem.* **2004**, *2004*, 4319−4322.
(89) Constable, E. C.; Housecroft, C. E.; Neuburger, M.; Schönle, J.; Zampese, J. A. The surprising lability of bis(2,2':6',2"-terpyridine)-chromium(III) complexes. *Dalton Trans.* **2014**, *43*, 7227−7235.
(90) Zare, D.; Doistau, B.; Nozary, H.; Besnard, C.; Guénée, L.; Suffren, Y.; Pelé, A.-L.; Hauser, A.; Piguet, C. Cr^{III} as an alternative to Ru^{II} in metallo-supramolecular chemistry. *Dalton Trans.* **2017**, *46*, 8992−9009.
(91) Scarborough, C. C.; Sproules, S.; Weyhermüller, T.; DeBeer, S.; Wieghardt, K. Electronic and Molecular Structures of the Members of the Electron Transfer Series $[Cr(tbpy)_3]^n$ (n = 3+, 2+, 1+, 0): An X-ray Absorption Spectroscopic and Density Functional Theoretical Study. *Inorg. Chem.* **2011**, *50*, 12446−12462.
(92) Scarborough, C. C.; Lancaster, K. M.; DeBeer, S.; Weyhermüller, T.; Sproules, S.; Wieghardt, K. Experimental Fingerprints for Redox-Active Terpyridine in $[Cr(tpy)_2](PF_6)_n$ (n = 3−0), and the Remarkable Electronic Structure of $[Cr(tpy)_2]^{1-}$. *Inorg. Chem.* **2012**, *51*, 3718−3732.
(93) Becker, P. M.; Forster, C.; Carrella, L. M.; Boden, P.; Hunger, D.; Slageren, J.; Gerhards, M.; Rentschler, E.; Heinze, K. Spin Crossover and Long-lived Excited States in a Reduced Molecular Ruby. *Chem. - Eur. J.* **2020**, *26*, 7199−7204.
(94) CIE (1932). *Commission internationale de l'Eclairage proceedings*; Cambridge University Press: Cambridge, 1931.
(95) Eysel, H. H. Absorptions- und Lumineszenzspektrum von Hexamminchrom(III)-salzen. *Z. Phys. Chem.* **1970**, *72*, 82−90.
(96) Kreidt, E.; Kruck, C.; Seitz, M. *Handbook on the Physics and Chemistry of Rare Earths*; Bünzli, J. C.-G., Pecharsky, V. K., Eds.; Elsevier: Amsterdam, 2018; Vol. *53*, pp 35−79.
(97) Suzuki, K.; Kobayashi, A.; Kaneko, S.; Takehira, K.; Yoshihara, T.; Ishida, H.; Shiina, Y.; Oishi, S.; Tobita, S. Reevaluation of absolute luminescence quantum yields of standard solutions using a spectrometer with an integrating sphere and a back-thinned CCD detector. *Phys. Chem. Chem. Phys.* **2009**, *11*, 9850−9860.
(98) Young, R. C.; Meyer, T. J.; Whitten, D. G. Electron transfer quenching of excited states of metal complexes. *J. Am. Chem. Soc.* **1976**, *98*, 286−287.
(99) Juris, A.; Balzani, V.; Barigelletti, F.; Campagna, S.; Belser, P.; von Zelewsky, A. Ru(II) polypyridine complexes: photophysics, photochemistry, eletrochemistry, and chemiluminescence. *Coord. Chem. Rev.* **1988**, *84*, 85−277.
(100) Farney, E. P.; Chapman, S. J.; Swords, W. B.; Torelli, M. D.; Hamers, R. J.; Yoon, T. P. Discovery and Elucidation of Counteranion Dependence in Photoredox Catalysis. *J. Am. Chem. Soc.* **2019**, *141*, 6385−6391.
(101) Ma, D.; Duan, L.; Wei, Y.; He, L.; Wang, L.; Qiu, Y. Increased phosphorescent quantum yields of cationic iridium(III) complexes by wisely controlling the counter anions. *Chem. Commun.* **2014**, *50*, 530−532.
(102) Henry, M. S. Prolongation of the Lifetime of the ^2E State of Tris(2,2'-bipyridine)chromium(III) Ion by Anions in Aqueous Solution. *J. Am. Chem. Soc.* **1977**, *99*, 6138−6139.

https://doi.org/10.1021/jacs.1c05971
J. Am. Chem. Soc. 2021, 143, 11843−11855

(103) Schoonover, J. R.; Strouse, G. F.; Omberg, K. M.; Dyer, R. B. Application of transient vibrational spectroscopies to the excited states of metal polypyridyl complexes. *Comments Inorg. Chem.* **1996**, *18*, 165−188.
(104) Bäppler, F.; Zimmer, M.; Dietrich, F.; Grupe, M.; Wallesch, M.; Volz, D.; Bräse, S.; Gerhards, M.; Diller, R. Photophysical dynamics of a binuclear Cu(I)-emitter on the fs to μs timescale, in solid phase and in solution. *Phys. Chem. Chem. Phys.* **2017**, *19*, 29438−29448.
(105) Boden, P.; Di Martino-Fumo, P.; Otto, S.; Seidel, W.; Heinze, K.; Gerhards, M. Transient FTIR spectroscopy after pump/pump vs. pump/dump excitation and temperature dependent luminescence investigations on a highly luminescent chromium(III) complex. *Phys. Chem. Chem. Phys.* **2021**, *23*, 13808−13818.
(106) Ando, H.; Iuchi, S.; Sato, H. Theoretical study on ultrafast intersystem crossing of chromium(III) acetylacetonate. *Chem. Phys. Lett.* **2012**, *535*, 177−181.
(107) Juban, E. A.; McCusker, J. K. Ultrafast Dynamics of ^{2}E State Formation in Cr(acac)$_3$. *J. Am. Chem. Soc.* **2005**, *127*, 6857−6865.
(108) Schrauben, J. N.; Dillman, K. L.; Beck, W. F.; McCusker, J. K. Vibrational coherence in the excited state dynamics of Cr(acac)$_3$: probing the reaction coordinate for ultrafast intersystem crossing. *Chem. Sci.* **2010**, *1*, 405−410.
(109) Johansson, J. O.; Kim, J.-W.; Allwright, E.; Rogers, D. M.; Robertson, N.; Bigot, J.-Y. Directly probing spin dynamics in a molecular magnet with femtosecond time-resolution. *Chem. Sci.* **2016**, *7*, 7061−7067.
(110) Arias-Rotondo, D. A.; McCusker, J. K. The photophysics of photoredox catalysis: a roadmap for catalyst design. *Chem. Soc. Rev.* **2016**, *45*, 5803−5820.
(111) Connelly, N. G.; Geiger, W. E. Chemical Redox Agents for Organometallic Chemistry. *Chem. Rev.* **1996**, *96*, 877−910.
(112) Kurihara, T.; Suzuki, T.; Wakabayashi, H.; Ishikawa, S.; Shindo, K.; Shimada, Y.; Chiba, H.; Miyashi, T.; Yasunami, M.; Nozoe, T. Electronic Structures and Oxidation Potentials of Some Azulene Derivatives. *Bull. Chem. Soc. Jpn.* **1996**, *69*, 2003−2006.
(113) Khusnutdinova, J. R.; Milstein, D. Metal−Ligand Cooperation. *Angew. Chem., Int. Ed.* **2015**, *54*, 12236−12273.
(114) Aboshyan-Sorgho, L.; Besnard, C.; Pattison, P.; Kittilstved, K. R.; Aebischer, A.; Bünzli, J.-C. G.; Hauser, A.; Piguet, C. Near-InfraredVisible Light Upconversion in a Molecular Trinuclear d−f−d Complex. *Angew. Chem., Int. Ed.* **2011**, *50*, 4108−4112.
(115) Jimenez, J.; Cerdan, L.; Moreno, F.; Maroto, B. L.; García-Moreno, I.; Lunkley, J. L.; Muller, G.; de la Moya, S. Chiral Organic Dyes Endowed with Circularly Polarized Laser Emission. *J. Phys. Chem. C* **2017**, *121*, 5287−5292.
(116) Zhang, D.-W.; Li, M.; Chen, C.-F. Recent advances in circularly polarized electroluminescence based on organic light-emitting diodes. *Chem. Soc. Rev.* **2020**, *49*, 1331−1343.
(117) Jiménez, J.-R.; Poncet, M.; Míguez-Lago, S.; Grass, S.; Lacour, J.; Besnard, C.; Cuerva, J. M.; Campaña, A. G.; Piguet, C. Bright Long-Lived Circularly Polarized Luminescence in Chiral Chromium(III) Complexes. *Angew. Chem., Int. Ed.* **2021**, *60*, 10095−10102.

https://doi.org/10.1021/jacs.1c05971
J. Am. Chem. Soc. 2021, 143, 11843−11855